Deliverable D4.4
Report on innovative decontamination process
30.4.2024 version Final

Dissemination level Public

Tomo SUZUKI-MURESAN

IMT Atlantique

4 Rue Alfred Kastler, 44307 Nantes, France

Email: suzuki@subatech.in2p3.fr

Tel: +33 2. 51. 85. 86. 71

Project acronym PREDIS	Project title PRE-DISposal management of radioactive waste	Grant agreement No. 945098
Deliverable No. D4.4	Deliverable title Report on innovative decontamination process	Version Final
Type Report	Dissemination level Public	Due date M44
Lead beneficiary IMT		WP No. 4

Main author Tomo Suzuki, IMT	Reviewed by Abdesselam Abdelouas, IMT, WP4 Leader	Accepted by Maria Oksa, VTT, Coordinator
Contributing authors Aditya Rivonkar, Tomo Suzuki, Abdesselam Abdelouas, IMT Atlantique; Thomas Carey, Anne Callow, NNL; Alban Gossard, CEA		Pages 42

Abstract

The report presents two technological advancements offering effective and sustainable solutions for managing metallic radioactive wastes: COREMIX Process and EASD® for chemical and electrochemical decontamination of metal surfaces (specifically SS304L and SS316 types), respectively. Evaluation of decontamination efficiency involved solution analysis (ICP-MS) and solid characterization (XRD, SEM/EDX, APT).

The COREMIX Process represents a chemical process for decontaminating metallic surfaces. This approach optimizes the use of high chemical concentrations to significantly reduce the number of required treatment cycles, resulting in substantial time and resource savings. Furthermore, the use of oxalic acid and potassium permanganate enables the removal of oxide layers, which is important for effective decontamination. The COREMIX-H Process also takes into account the additional cleaning step with hydrogen peroxide for effluents rich in oxalic acid that meets the recommendations of waste acceptance criteria.

The Electrolytically Assisted Surface Decontamination (EASD®) represents a significant advancement in electropolishing technology, offering a rapid and precise method for removing radioactivity from metal surfaces. This technology, developed in collaboration with C-Tech Innovation Ltd., enables in-situ decontamination of nuclear sites during their decommissioning phase. EASD® Gel is a technology that uses a gel-based electrolyte to target specific contamination zones on metal surfaces without generating new chemical waste.

Keywords
Metallic radioactive waste, decontamination, chemical decontamination, electrochemical decontamination

TABLE OF CONTENTS

1   Introduction

The nuclear industry can play a crucial role in providing low-carbon energy, but it also generates significant volumes of radioactive waste which has to be storage over very long time periods (10–1000's years). As the demand for nuclear energy grows, so does the volume of radioactive waste generated, calling for a critical examination of traditional decontamination methods. Conventional decontamination techniques, such as mechanical and thermal methods, often face limitations in effectively removing radionuclides. Other techniques such as chemical and laser techniques are also effective but generate secondary wastes which are hard to manage. This necessitates the development of innovative decontamination approaches that are both efficient and environmentally friendly.

Metals are essential components of the nuclear industry, providing durability for components that must withstand extreme conditions such as high temperatures, pressure, and radiation. Austenitic stainless steel and Ni-alloys, for example, are used in reactor primary circuit systems due to their strength and corrosion resistance. Corrosion resistance is particularly important in the nuclear industry due to the presence of radioactive elements. Zirconium-based materials are also used for cladding nuclear fuel rods due to its corrosion resistance in water and its ability to absorb neutrons, a critical property for sustaining nuclear chain reactions. Metals also facilitate efficient heat transfer in nuclear reactors, an essential function for maintaining reactor operation.

Nuclear metallic waste originates from reactor components that have been exposed to radioactive effluent process streams. The amount of metallic waste generated by nuclear power plants depends on factors such as plant size and design. A standard 1,000-megawatt nuclear plant is estimated to produce 20,000 to 30,000 metric tons of metallic waste over its lifetime [1–3]. France's nuclear plants are expected to generate approximately 1.3 million metric tons of metallic waste alone [4].

Metallic waste constitutes a large proportion of that arising from the nuclear energy industry, therefore methodologies for minimisation are desirable. Radioactive metallic waste comes from various sources and is categorized as Low-Level Waste (LLW) and Intermediate-Level Waste (ILW) depending on its associated radioactivity. Efficient management of nuclear waste, including metallic waste, is crucial for human health, environmental protection, and public trust in the nuclear industry. Challenges include varying waste volumes, radioactivity levels, and the associated risks. Proper disposal, storage, and compliance with regulations are essential for safety, environmental protection, and effective waste management. Public perception also plays a significant role in managing radioactive waste.

1.1   Origins of radioactive contamination and optimal decontamination approaches

The metallic components are crucial elements of nuclear power plants, typically stainless steels and Ni-alloys, chosen for mechanical strength, corrosion resistance, and durability in harsh conditions [5–8]. Despite their corrosion-resistant properties, these metals may undergo some corrosion over the operational life of the plant (decades), caused by the high-temperature and pressure environments. Corrosion can facilitate the activation and uptake of radionuclides into the surface oxide layers of the metal components [5,9–11]. In pressurised water reactors (PWRs), contaminating radionuclides have two main sources. The first is the activation of corrosion products like cobalt, iron, and nickel that dissolve and enter the primary circuit water. Neutron exposure in the system can transform stable isotopes in these corrosion products into radioactive isotopes, contributing to contamination. The second source is the deposition of fission products released in the event of

cladding failure. These fission products, byproducts of nuclear reactions, can deposit onto the metal oxide layer, especially in complex geometries like tube bends.

Spent nuclear fuel reprocessing plants also employ a range of corrosion resistant metals. Nitric acid-based processed are commonly used in these plants for dissolving nuclear fuel and isotopic separation [12–18]. As a result, these metals develop a unique type of corrosion layer, typically just a few tens of nanometres thick. This layer, while providing a protective barrier against further corrosion, also becomes an integral part of the metallic waste stream. It becomes particularly enriched with fission products that are dissolved along with the spent nuclear fuel, and become embedded in surface layers, posing a challenge for decontamination and disposal. The presence of these radionuclides in the corrosion layer necessitates decontamination of these systems to any hands-on dismantling, waste segregation and management.

Decontamination techniques are employed to mitigate radioactive contamination, aiming to remove the radioactive oxide layer and any diffusion of radioactivity from the bulk metal. Considering the complex geometries of the primary circuit, prevalent chemical techniques, particularly liquid washing with specific chemical solutions, prove commonly effective. These methods achieve thorough decontamination without necessitating physical modifications to components, addressing challenges posed by intricate structures like steam generators.

On surfaces that are more accessible, one can employ electrochemical and/or gel decontamination methods, providing notable advantages, including the reduction of secondary waste. Electrochemical methods involve utilizing electrical currents to drive decontamination reactions, while gel-based techniques utilize specialized chemicals to enhance the contact time and effectiveness of the decontamination process. These approaches not only contribute to efficient decontamination but also address concerns related to waste generation, making them practical and environmentally favourable choices for certain scenarios.

1.2 Overview of Decontamination Methodologies

Decontamination is the process of removing contaminants from surfaces using a variety of methods, including washing, heating, chemical treatment, electrochemical processes, or mechanical means. It is commonly used in nuclear facilities to clean equipment and components, such as the exteriors and interiors of buildings, equipment, pavements, and vehicles. In some instances, decontamination may also involve removing radioactivity that is deeply embedded within materials.

Within the nuclear industry, various decontamination methods are employed, encompassing:

1) Mechanical Methods: This involves physically scrubbing or scraping contaminated surfaces to eliminate radioactive materials. Typically applied to large, flat surfaces or areas with loose contamination, tools such as brushes, scrapers, high-pressure water jets, and techniques like high-pressure liquid jetting (including high pressure and ultra-high pressure), dry ice blasting, laser-based cleaning, nonthermal plasmas, low-pressure arc plasma, supercritical fluid cleaning, and air-blast cleaning are utilized [19–28].

2) Chemical Methods: Chemical decontamination methods involve utilizing processes such as dissolution, oxidation/reduction, and complexation to liberate contaminants from surfaces into a liquid waste stream. These methods encompass techniques such as reagent washing, foam decontamination, chemical gel and strippable coatings [26–28]. The reagents employed for chemical decontamination approaches include water alone or in combination with soap, surfactants, acids, bases, chelating agents, or redox-active agents. Foams, gels, or pastes are employed to extend the contact time between the contaminant and the reagent, thereby enhancing contaminant removal.

3) Electrochemical methods: these work in a similar way to chemical decontamination processes. Rather than utilising chemical reagents to dissolve contaminated surfaces, an applied electrical current is used instead.

4) High-Temperature Cleaning, also recognized as thermal decontamination, employs elevated temperatures to volatilize or break down contaminants. By heating the contaminated surfaces, this method causes radioactive materials to vaporize, effectively eliminating them from the surface. Typically applied to metallic surfaces capable of withstanding high temperatures, thermal decontamination is a commonly employed technique [26–28].

5) Ultrasonic Cleaning utilizes high-frequency sound waves to generate microscopic bubbles in a liquid cleaning solution [28]. These bubbles collapse near the contaminated surface, creating an intense scrubbing action that dislodges and removes radioactive materials. Particularly effective for small, intricate, or hard-to-reach objects, ultrasonic cleaning offers a meticulous decontamination process.

6) Biological Decontamination involves the utilization of living organisms, such as bacteria or fungi, to break down or transform radioactive contaminants [28]. Certain microorganisms possess the ability to absorb, metabolize, or immobilize radioactive substances. Research and development efforts continue to explore and refine biological decontamination methods for specific application.

Various decontamination methodologies were selected for this work based on the specific types of wastes targeted for treatment, encompassing chemical immersion, electrochemical, and gel decontamination methods. The National Nuclear Laboratory (NNL) focused on Electrolytically Assisted Surface Decontamination (EASD) techniques, while IMT Atlantique concentrated on chemical methods on Chemical Oxidation Reduction with nitric permanganate and oxalic acid MIXture (COREMIX). This report follows the previous deliverable 4.3, led by CEA, which focused the development of vacuumable gels for the decontamination of metallic surfaces. A comprehensive literature review of existing chemical decontamination methods preceded the selection of one method for optimization target. The objective is to streamline processes, reduce costs, minimize waste volumes, and improve the overall sustainability of the decontamination process.

2 Sample Preparation and Characterization

The study employed two distinct sets of samples which replicated the metallic waste originating from varying environments of nuclear facilities. Stainless steel 316 samples, mimicking the conditions of a nuclear power plant's primary circuit, were prepared by the Hungarian organization Social Organization for Radioecological Cleanliness (SORC). Simultaneously, stainless steel 304L samples, mirroring the nitric acid-grade stainless steel used at the reprocessing plants at Sellafield in the UK, were prepared by the UK's National Nuclear Laboratory (NNL). Both SORC and NNL are collaborating partners within the WP4 of the project. By utilizing these diverse sample sets, the study gained a comprehensive understanding of materials from different aspects of nuclear facilities, providing valuable insights for the project's research objectives.

Both sets of samples underwent characterization using various methods to ensure that the oxide layers accurately reflect the conditions encountered in an industrial setting. This examination is crucial for validating the representativeness of the samples and enhancing the relevance of the study to real-world scenarios.

2.1 Stainless steel 316

2.1.1 Preparation

SORC procured and prepared surrogate samples of stainless steel 316 for experimentation. The oxidation process was conducted using induction heating at high temperatures ranging from 600 to 800°C. Distilled water/boric acid solutions were then passed over the samples for a duration of 8 hours. Some SS-316 samples were exposed to boric acid solutions with concentrations set at 0 g/L, 1 g/L and 15 g/L. The inclusion of boric acid aimed to replicate the chemistry of water in the primary circuit of a Pressurized Water Reactor (PWR). Experimental setup details can be found here D. Horvath [29] and R. Katona [30]. Figure 1 illustrates the oxidized sample resulting from this experimental process.
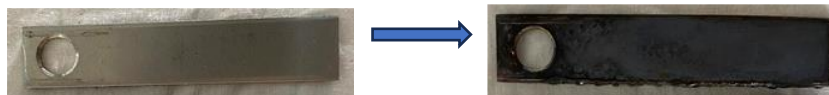

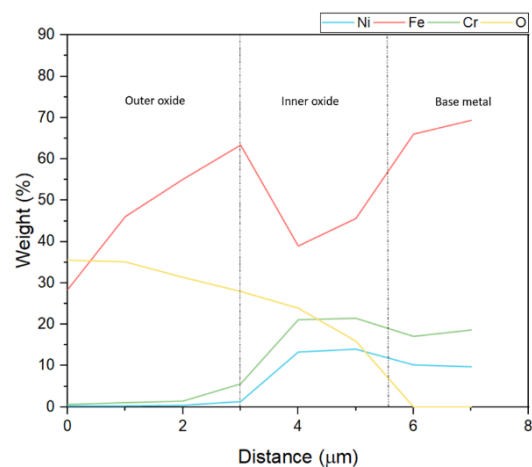*Figure 1 Evolution of SS316 samples through the oxidation process*

2.1.2 Characterization of SS316

The analysis of the oxide layers on the samples involved the utilization of Scanning Electron Microscope with Energy Dispersive Spectroscopy (SEM-EDX) and X-ray diffraction (XRD) techniques.

The examination of the oxide cross-section through SEM revealed an average thickness of 5 µm, as illustrated in Figure 2A. For the oxide analysis, EDX was employed, using the preset line detection tool with a 1 µm spacing between measurement points. The analysis unveiled a multi-layered oxide structure, as depicted in Figure 2B. The outer layer exhibited an enrichment in Fe, while the inner layer displayed an enrichment in Cr and Ni. These findings align with observations made by Panter et al. [11] and McGrady [10], who similarly noted the presence of a multi-layered oxide structure in their studies.
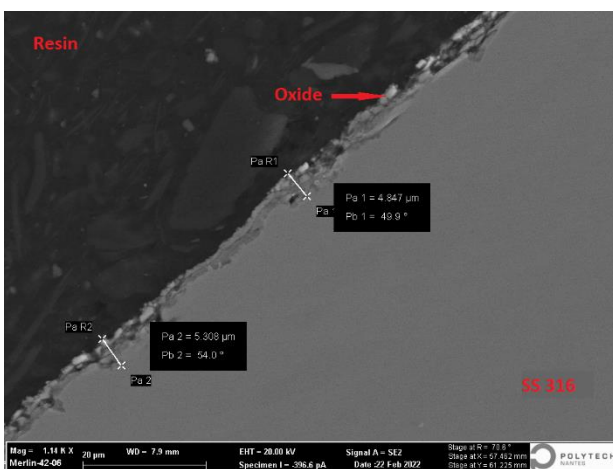
(A) SEM image of oxide layer   *(B) EDX profile of oxide layer*

Figure 2 SEM and EDX profile of oxidized SS-316 in 15g/L boric acid prepared by SORC

In instances of varying boric acid concentrations, it was observed that increasing concentration correlated with a reduction in the thickness of the oxide layers. For samples oxidized in the same batch, the oxide thickness was approximately 9.65 μm with 0 g/L boric acid and 5 μm with 15 g/L boric acid. These findings align with previous literature studies examining the effects of boric acid [31,32]. Zhang et al. [32] reported minimal corrosion rates of SS316 in boric acid solutions and observed the rapid formation of a passive layer on the metal surface. The presence of boric acid during the oxidation process did not significantly alter the multi-layered nature of the oxide formed on the SS316 samples. The oxide layer continued to exhibit the characteristic composition, featuring an inner barrier layer enriched in Cr and an outer layer enriched in Fe oxide.
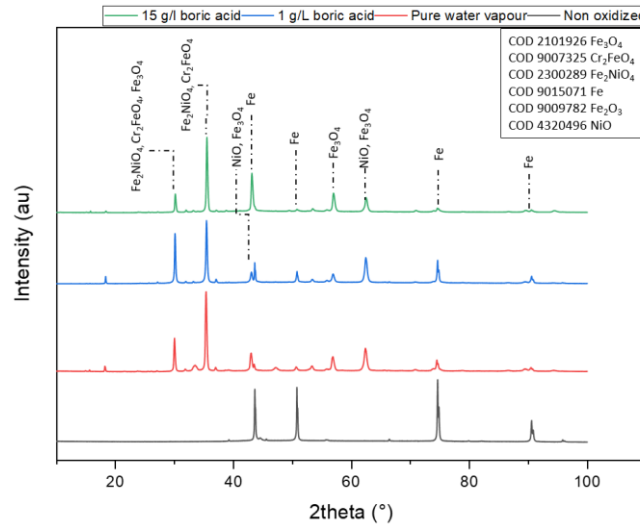

Figure 3 XRD profile of oxidized SS316 as a function of different concentrations of boric acid

Upon X-ray diffraction (XRD) analysis of the oxide surface, various oxides of Ni, Fe, and Cr, such as Fe_3O_4, Fe_2O_3, NiO, and Cr_2FeO_4, were identified, as illustrated in Figure 3. These oxide compositions are consistent with observations in existing literature [10,11,33], reinforcing the reliability of the study's findings.

The influence of boric acid on the XRD profiles of the oxide samples was noticeable, although the changes were relatively small. The composition of the oxide layer appeared unaffected by the varying concentration of boric acid. Regardless of the boric acid concentration, the oxidized pieces consistently exhibited the presence of NiO, Fe_2NiO_4, Fe_3O_4, among others.

While there was a subtle difference in the intensity of the peaks, it is crucial to highlight that the observed changes in the XRD profiles were relatively minor. This suggests that the impact of boric acid on the oxide composition may be subtle if any.

2.2 Stainless steel 304L

2.2.1 Preparation

The National Nuclear Laboratory (NNL) developed a controlled boiling-acid process to create SS-304L samples that mimicked the conditions found in the Sellafield reprocessing plant (corrosion in contact with a hot, concentrated nitric acid). Cuboid samples (~50 x 10 x 10mm) were initially prepared in this work, but these were later replace by circular disk samples (32mm OD, 3mm depth) as this geometry had advantages for more characterisation with a wider range of techniques. All samples were prepared by boiling under reflux (Figure 4) in a simulant reprocessing liquor (approximately 120 °C), consisting of 8 M HNO_3 and a range of metal nitrates the concentration of which are shown in Table 1. These elements contain fission products and other elements found in the course of fuel reprocessing activities. This deliberate addition aims to create a chemical setting that closely mirrors the conditions observed during actual processes, contributing to the accuracy and relevance of the experimental setup to that expected on nuclear sites. The coupons were removed from solution and allowed to dry in a desiccator for a month. This resulted in a dark oxide film which had a rough appearance following grain dropping during corrosion.
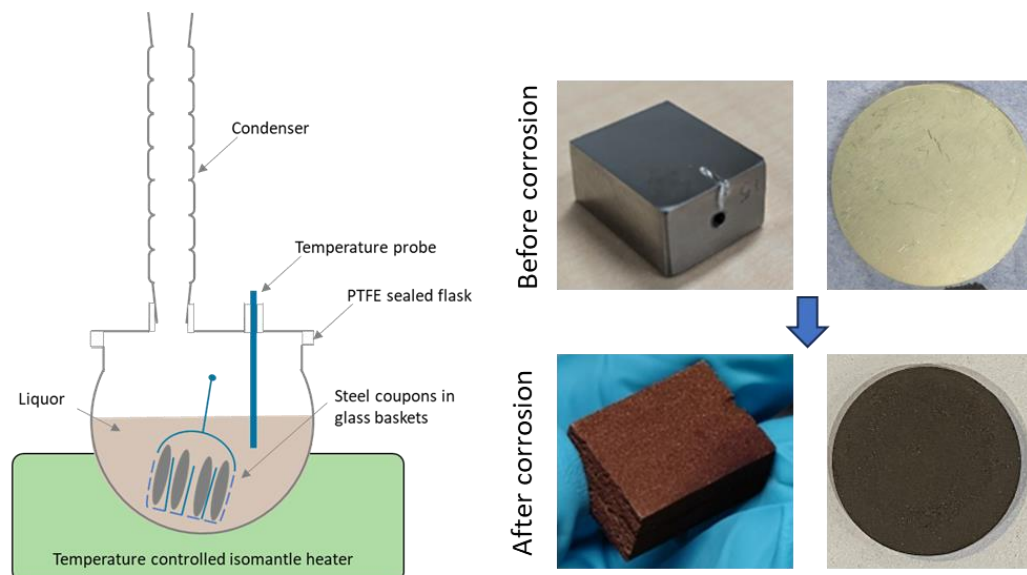

Figure 4: Left – diagram of the experimental set-up and Right – 304L stainless steel coupons before (top) and after (bottom) corrosion in simulant reprocessing liquor.
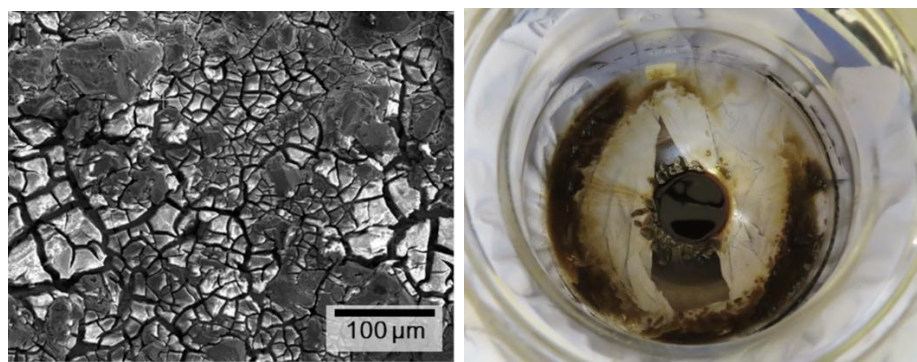

Figure 5: Left: SEM image of the corroded steel surface (Mag: 207 x, SE Mode, 15 kV: 1.6 nA probe). Right: Deposits left behind in the corrosion test vessel after 10 days.

Table 1: Concentration of elements in the simulant reprocessing liquor

Element	Concentration in simulant	
	mol/L	g/L
N (from NH4)	1.4962	20.95
Na	0.0199	0.46
Al	0.0286	0.77
P	0.0378	1.17
K	0.0199	0.78
Cr	0.0614	3.19
Fe	0.2144	12.01
Ni	0.0415	2.45
Rb	0.0192	1.65
Sr	0.0437	3.85
Y	0.0227	2.02
Zr	0.1874	17.05
Mo	0.1471	14.12
Re	0.03	5.58
Ru	0.0459	4.64
Rh	0.0106	1.09
Pd	0.0425	4.51
Te	0.0146	1.87

2.2.2 Elemental Mapping of the Contaminated 304L Surface using SEM/EDX

Scanning electron microscopy (SEM) and energy dispersive x-ray spectroscopy (EDX) were used to produce elemental maps of the surface of the 304L coupon. A surface layer of dried on liquor was present (Figure 5) which had regions of different elemental composition (Figure 6), with some areas rich in Zr and P, others with redeposited corrosion products (Fe, Cr), or with liquor constituents (Gd, Ce, Cs). It is suggested that this outer layer formed as the simulant liquor dried and left behind solid deposits, with different regions forming from elements of differing solubility. It was noted that sludge formed in the solution during corrosion, so the layer of contamination on the sample surface may have originated in a similar way as elements from the liquor precipitated as oxide or hydroxide phases.
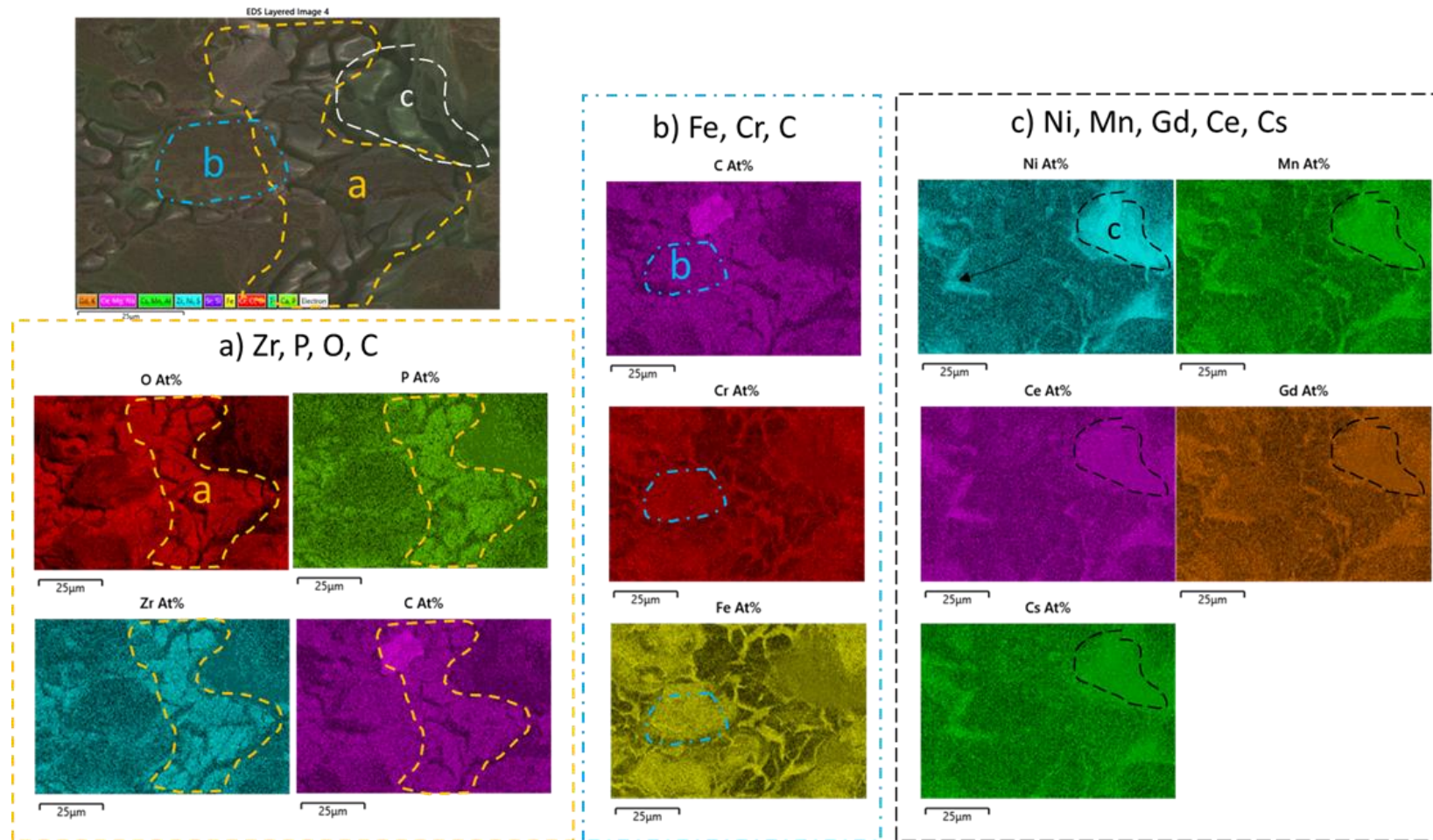
Figure 6: EDX elemental maps of the sample surface of 304L corroded by boiling for 10 days in simulant reprocessing simulant liquor

2.2.3 APT Characterisation of 304L Contamination Layer

Specimens of 304L stainless steel were characterised using atom probe tomography (APT). The coupon was coated with Pt-Pd before using a Helios FIB-SEM to prepare needle-shaped specimens using a standard APT lift-out procedure (Figure 15) [34]. A small amount of Pt-Pd capping layer was deliberately left intact on the needle (~ 60 - 80 nm) so that the oxide layer would be captured within the APT analysis volume. Data was acquired at the University of Oxford, UK using a LEAP 5000XR Local Electrode Atom Probe microscope. Laser-pulsing mode was used to reduce stress on the sample, with run conditions of 50 K, 60 pJ laser energy, and 0.5 % detection rate. A relatively low laser pulse frequency of 65 kHz, to avoid mass spectrum 'wrap around' of the heavier elements within the contaminated oxide layer and capping layer.
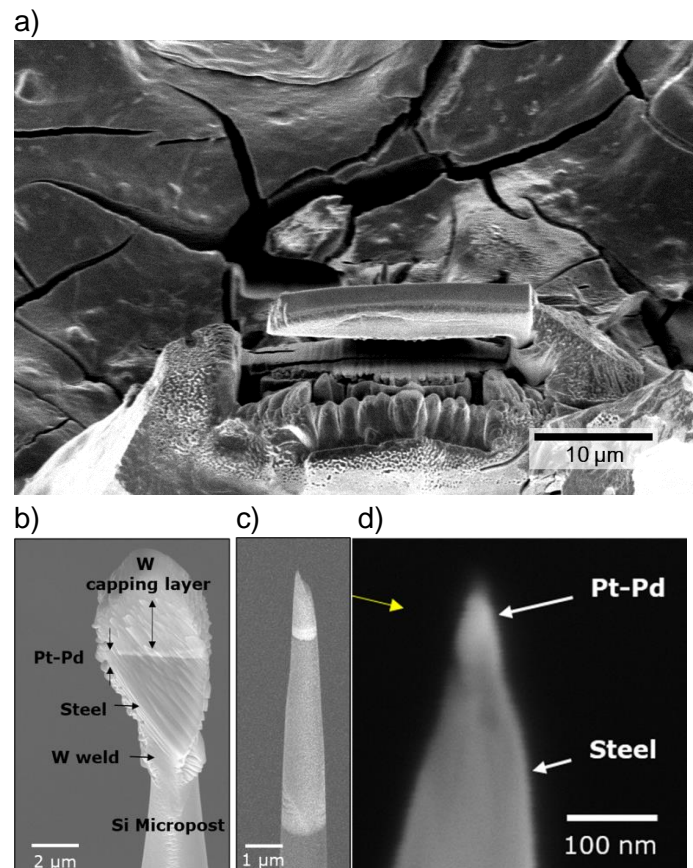

Figure 7: APT sample preparation carried out using the Helios FIB-SEM) – a) sample lift out, b) mounting, c) polishing and d) capping.

The APT data showed that the metal-oxide interface was 'wavy' and heterogeneous, with an outer Fe-rich, inner Cr-rich layer, an oxygen diffusion region into the metal (Figure 8). The metal-oxide interfacial region was enriched with native nickel due to the preferential dissolution of iron into solution during corrosion. Depth profiling using a proximity histogram located at the metal oxide interface (~28 at% oxygen) was carried out, Figure 10. This proximity histogram showed an oxide layer of approximately 10 – 15 nm in thickness, with a 30 nm interfacial region. Contamination was present in the oxide and metal-oxide interface, and within the oxygen diffusion region in the underlying metal. Importantly, the depth profile indicated that contamination was not present within the metal below 2 at% oxygen.

Care should be taken when interpreting the proximity histogram in Figure 10, because it is plotted around a complex interface. The depth shown on the distance axis refers to the distance away from

the curved interface, rather than referring to the contamination depth from the material surface. As measured from the top of the APT dataset, the contamination depth was approximately 80 nm, although only a few datasets were obtained. It is possible that the steel coupon had deeper oxygen diffusion should more APT datasets have been acquired from other areas, and therefore a deeper contaminated region. The data acquisition was also stopped close to the end of the oxide, so that the tip in Figure 8 (a) was analysed in a separate session to determine if any oxide remained. The result of this is shown in Figure 9, where an additional 10 – 15 nm of oxide was found. This dataset was also used as an additional dataset from which to derive a steel matrix composition in Table 2.
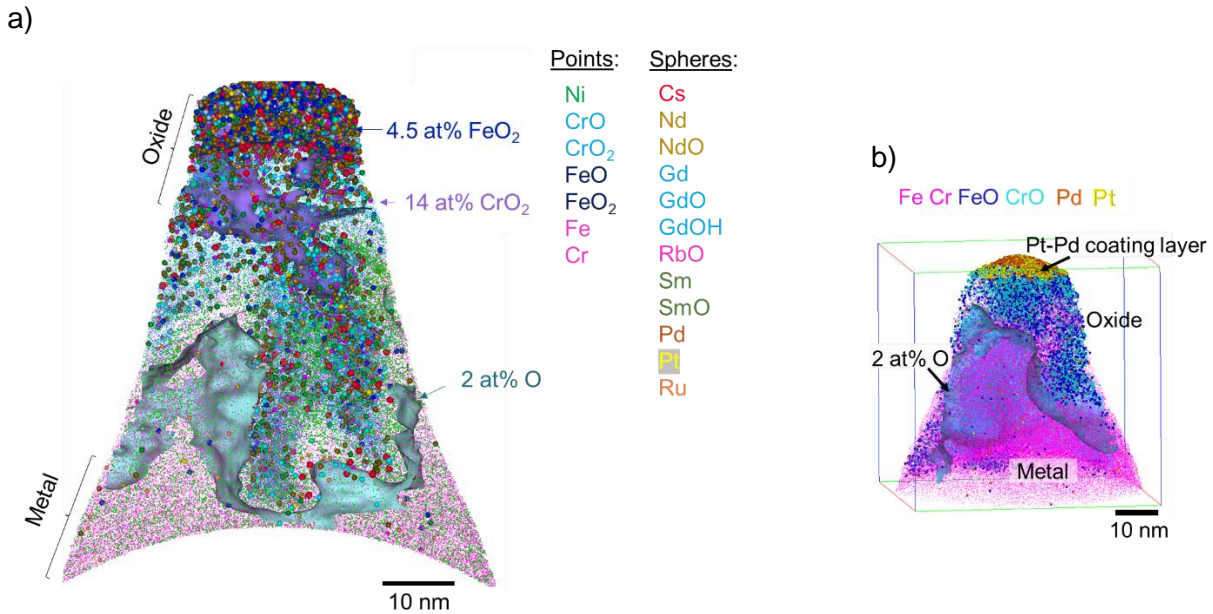

Figure 8: Two datasets from APT characterisation of the corrosion layer on 304L stainless steel, a) shows the iron rich and inner chromium rich oxide layers along with the contamination. The data in b) shows the Pt-Pd capping layer in-tact, showing the extent of the oxide.
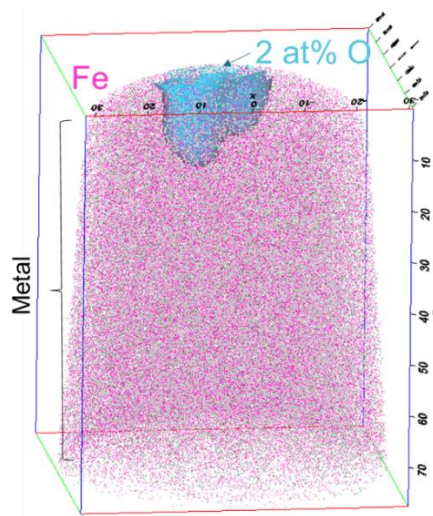

Figure 9: A second data acquisition performed on the same tip as shown in Figure 8, to verify the oxide depth.

Iso-concentration surfaces were used to extract metal and oxide layers, so that compositional analysis could be carried out on these regions in isolation. The results shown in Table 2 demonstrate that the oxide was contaminated up to a few at% with elements from the simulant liquor including Cs, Gd, Nd, Pd, Rb, Ru, Sm, V and Zr.

The Cr-rich inner oxide was non-stoichiometric which is agreement with the proximity histogram. If a stable oxide phase were present, it would be very narrow (~1 nm or less) as the oxygen plateau in Figure 10 did not have a discernible overlap with the chromium maximum (between 5 – 10 nm on the horizontal axis). The average steel composition from the matrix was found to be in agreement with the values expected for 304L stainless steel.

For completeness of information, the APT mass spectra and their ranges are shown for the Cr-rich oxide and the underlying metal (<2 at% oxygen) in Figure 11 and Figure 12. The absence of elements from the composition does not necessarily exclude them, as some elements in the liquor had overlapping peaks with the constituents of the steel oxide and therefore low concentrations of some elements were more challenging to quantify.

Overall, these results suggest that contamination would not be present beyond the oxygen diffusion layer, so that removing the top few hundred nanometres of material would provide adequate decontamination. Further work would be required to understand the depth of the oxygen diffusion region at crack tips ahead of inter-granular corrosion at grain boundaries. Since the contamination was associated with oxygen diffusion, it could reasonably be suggested that corroded grain boundary cracks would allow deeper contamination due to enhanced diffusion of oxygen along grain boundaries. These cracks can penetrate up to a whole grain width, therefore decontamination methods that remove the topmost layer of metal grains (tens of microns, alloy dependent) would be sufficient to remove a large portion of the contamination from the target material.
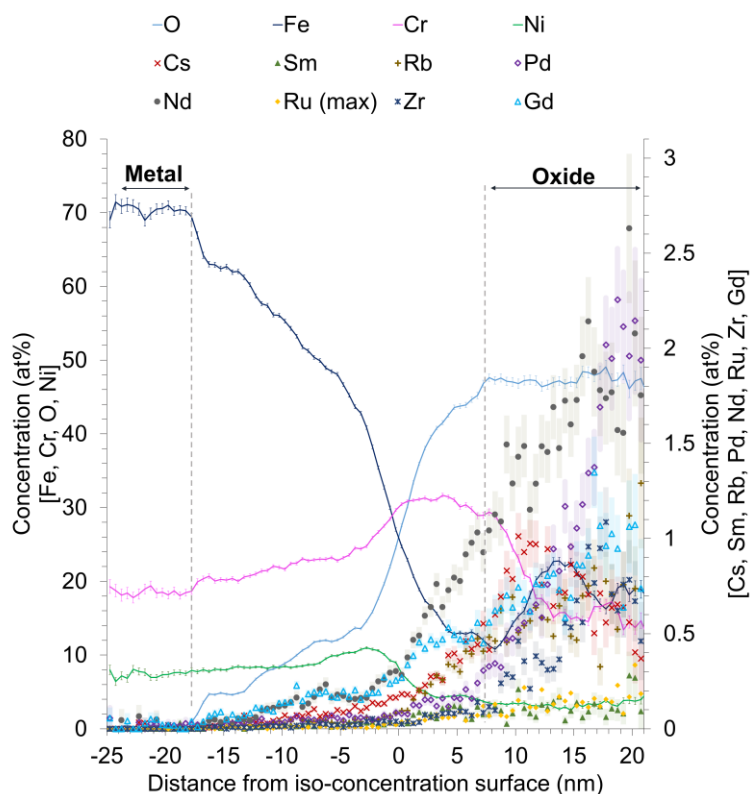

Figure 10: Proximity histogram defined using a 28 at% oxygen surface, showing the metal-oxide interface region of 304L corroded in simulant reprocessing liquor.

Table 2: Composition of the oxide layers and metal from APT analysis.

Element	Fe-rich layer	S.D.	Cr-rich layer	S.D.	Metal	S.D.
C	0.57	0.19	0.72	0.15	0.11	0.01
Co	0.28	0.18	0.29	0.03	0.30	0.03
Cr	13.5	10.25	31.57	1.43	18.2	0.11
Cs	0.41	0.02	0.31	0.25	-	
Cu	0.22	0.01	0.22	0.02	0.28	0.01
Fe	14.6	6.83	8.69	1.48	68.8	0.95
Gd	1.19	0.38	0.61	0.10	-	
Mn	0.29	0.08	0.96	0.05	1.34	0.03
Mo	2.27	0.02	1.14	0.15	1.48	0.39
Nd	2.58	0.92	1.77	0.27	-	-
Ni	5.04	1.42	2.73	0.62	7.0	0.16
N	-	-	-	-	0.10	0.03
O	52.7	2.90	48.6	1.26	1.69	0.26
P	-	-	-	-	0.02	0.00
Pd	0.48	0.01	0.19	0.03	-	-
Pt [a]	0.63	0.71	-	-	-	-
Rb	1.13	0.70	0.63	0.19	-	-
Ru (max)	0.41	0.04	0.26	0.04	-	-
Si	0.19	0.09	-	-	0.64	0.06
Sm	0.10	0.02	-	-	-	-
V	0.29	0.06	0.37	0.02	0.06	0.01
Zr	3.09	2.28	0.89	0.13	-	-
Datasets	2		2		3	

Fe-rich layers extracted using 1.8 - 4.5 % (ionic) FeO_2 iso-concentration surfaces. Cr-rich layers extracted using 10.0 – 14.0 % (ionic) CrO_2 iso-concentration surfaces. Metal extracted from 3 datasets, using 2 at% O iso-concentration surfaces.

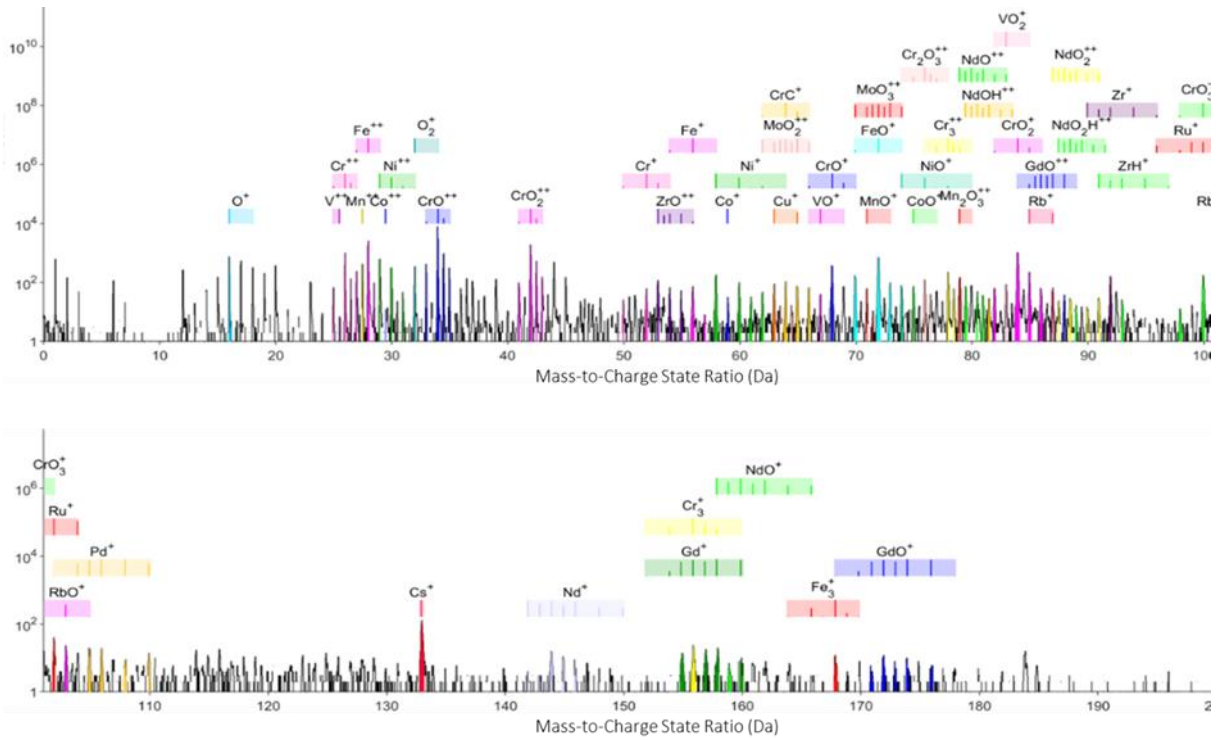[a] From the Pt capping layer, and not the liquor.

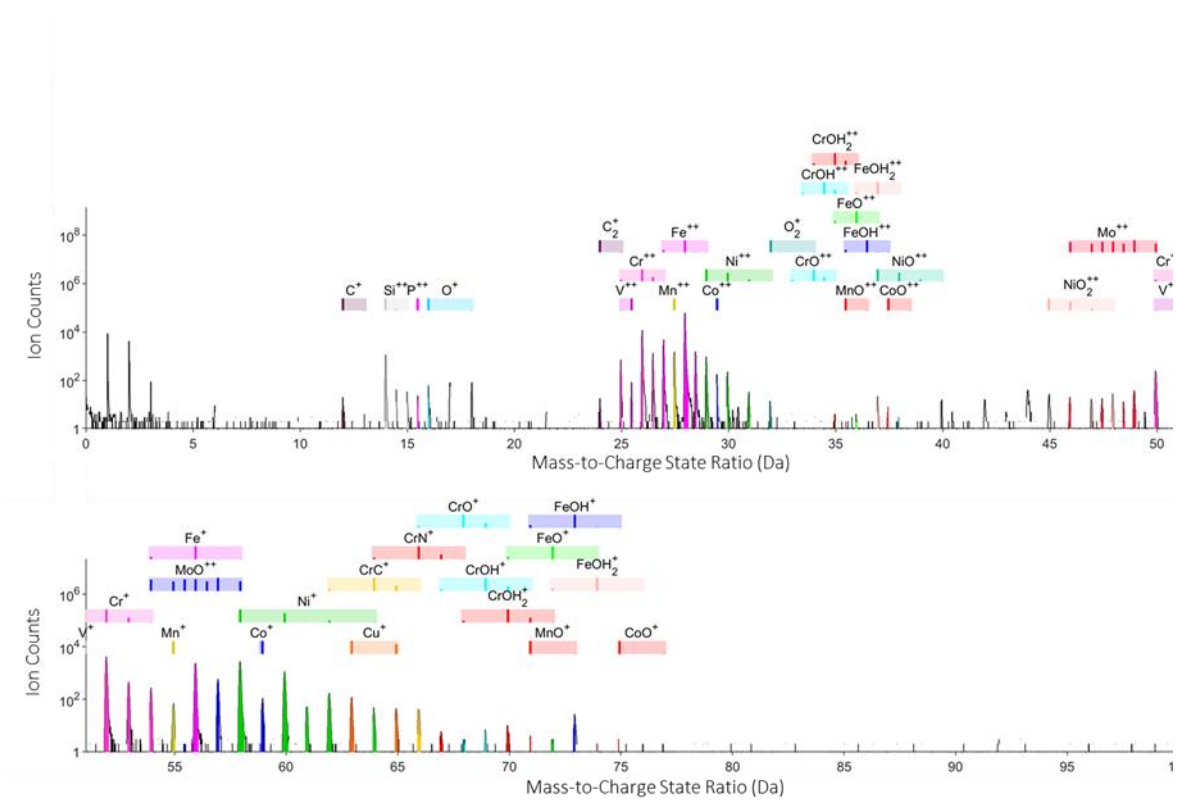Figure 11: Cr-rich oxide APT mass spectrum and ranging.

Figure 12: Metal (< 2 at% oxygen) APT mass spectrum and ranging

3 Chemical Oxidation Reduction with nitric permanganate and oxalic acid MIXture (COREMIX)

## 3.1 Introduction on the general methodology

The COREMIX process is derived from the Chemical Oxidation Reduction Decontamination (CORD) process renowned globally for its effectiveness and simplicity, this method is distinguished by its minimal generation of waste. The process can be broken down into 4 blended steps.

1. **Oxidation step**: In this step a mixture of 3mM nitric acid and 15mM potassium permanganate is used, and it is applied at 80°C for 3 hours. This step allows for the conversion of chromium from the insoluble Cr_2O_3 form to the highly soluble $HCrO_4^-$ according to the equation 1

$$Cr_2O_3 + 2MnO_4^- + H_2O \rightarrow 2HCrO_4^- + 2MnO_2 \qquad 1$$
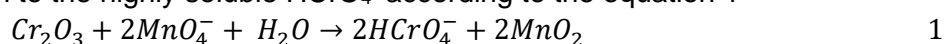
   During this step, a manganese dioxide (MnO_2) precipitate is formed.

2. **Reduction step**: Oxalic acid is added to reduce the remaining $KMnO_4$ to Mn^{2+} according to equation 2

$$2MnO_4^- + 5H_2C_2O_4 + 6H^+ \rightarrow 2Mn^{2+} + 10CO_2 + 8H_2O \qquad 2$$
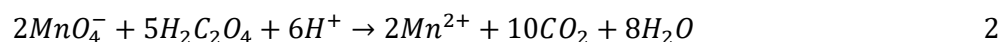
   The oxalic acid also dissolves the MnO_2 precipitate that is formed in the previous step. A total of 1.7 times the concentration of $KMnO_4$ is utilised in this step.

3. **Decontamination step**: Excess oxalic acid (18.5mM) is added to perform the decontamination reaction that involves the dissolution of Fe_3O_4 according to equation 3

$$Fe_3O_4 + 4H_2C_2O_4 \rightarrow 3FeC_2O_4 + 4H_2O + 2CO_2 \qquad 3$$
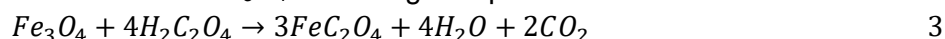
   In practice, steps 2 and 3 are combined together and applied at 80°C for a total of 3 hours.
   These steps comprise of one cycle of the process. Multiple cycles of the process can be applied to reach the target level of decontamination. No additional rinsing or cleanup is required in between the steps or in between two cycles.

4. **Cleanup step**: At the end of each cycle, the effluent is rich in oxalic acid which needs to be destroyed prior to treatment of the effluent. This is achieved by adding 0.1M hydrogen peroxide and heating the system for 24 hours, once again at 80°C. This process is known as the COREMIX-H (Chemical Oxidation REduction using nitric permanganate and oxalic acid MIXture with Hydrogen peroxide treatment) and can be applied at the end of each cycle or after all the cycles depending on the system volume. The effluent is now available for further treatment, either using ion exchange resins or a 2-step precipitation protocol (COREMIX-HP).

In comparison to the traditional CORD process, the COREMIX process distinguishes itself by its simplified system setup, eliminating the need for specific resins in CORD reagent preparation and a UV source. This streamlined design simplifies the application of the process, leading to cost savings. Furthermore, when combined with the precipitation process for effluent treatment (COREMIX-HP), it not only simplifies overall operations but also significantly reduces the volume of final waste. This integrated approach not only improves the decontamination process's efficiency but also highlights its potential to minimize environmental impact and waste generation.
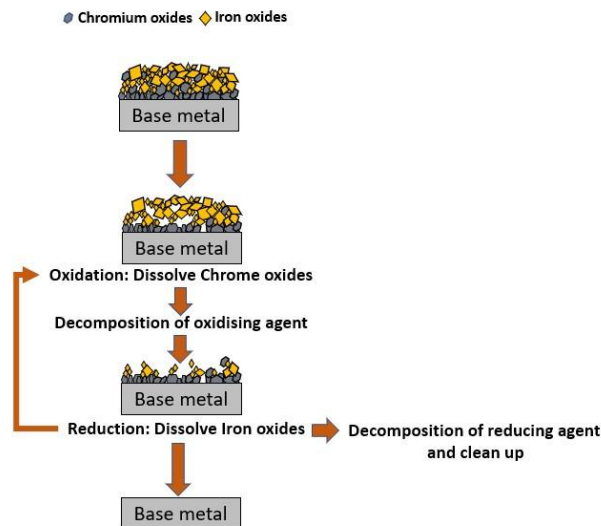The COREMIX process can be summarized in the Figure 13.

Figure 13 Operating principle of the COREMIX process, modified from Hitachi-GE Nuclear Energy, Ltd.'s [35], description of the CORD process which follows a similar chemistry

3.2 Methodology: Parameters for COREMIX Chemical decontamination optimization

Detailed experimental procedure utilizing COREMIX process, presented here, is provided in Rivonkar *et al.* [36], which was published as part of the PREDIS project framework. This article not only introduces the COREMIX process (as a variant of the CORD process) but also explores several steps and conditions crucial for optimizing its implementation.

Certain parameters have been identified and tested for optimization in order to improve the effectiveness of the treatment methods. These parameters include:

3.2.1 Concentrations

Adjusting chemical solution concentrations can impact efficiency, considering system compatibility and final resin requirements. It may also influence the duration of contact between the solution and the sample. The parameter was extensively tested, specifically exploring the effects of varying concentrations of $KMnO_4$ and HNO_3 to determine the most efficient solution with minimal volume and contact time. Similar investigations were conducted for oxalic acid concentration. Initially, concentrations from literature [9,37] included 6.3mM $KMnO_4$ in 3mM HNO_3, followed by 15mM oxalic acid, serving as the reference point. However, an increase in oxalic acid concentration would require higher H_2O_2 concentration for degradation, resulting in a substantial environmental impact according to LCA study feedback. Consequently, the baseline oxalic acid concentration was reduced to 10mM. Concentrations were then varied, with $KMnO_4$ ranging from 2mM to 6.3mM and 15mM, and oxalic acid ranging from 5.3mM to 10mM and 18.5mM. It's worth noting that the HNO_3 concentration was altered in tests involving powders, but it was determined to be optimal at 3mM also supported by the findings of Jung et al. [38].

3.2.2 Contact times

Optimizing the duration of contact between the solution and surfaces is critical for the decontamination process. Efficient results can be achieved with the same solution volume through careful adjustment of contact times. Solution temperature and concentration are influential factors

affecting the necessary contact times. In the experiments, contact times were varied for different solution concentrations to determine the minimum required time for effective decontamination. The objective was to enhance efficiency and reduce energy consumption. Ocken suggests an ideal contact time per cycle step between 4-6 hours [9]. Therefore, with the aim to minimize contact time, an initial baseline of 4 hours was utilized.

3.2.3   Chemical composition

Modifying the composition of chemicals in decontamination processes can enhance their effectiveness, such as changing the oxidation step within the COREMIX process, while considering the Waste Acceptance Criteria (WAC). The oxidation step in the COREMIX process offers two application methods.

a) **Nitric Permanganate** (NP): This involves a mixture of nitric acid and potassium permanganate, known as the nitric permanganate process (NP). NP exhibits strong oxidizing properties at a low pH of 2-3, making potassium permanganate highly effective in breaking down contaminants. However, it is crucial to acknowledge that the lower pH and the presence of nitric acid in NP render the solution more corrosive compared to alternative decontamination agents like Alkaline permanganate (AP) [9]. Choosing NP as a decontamination method involves a trade-off between its robust oxidation capabilities and the corrosive nature associated with its lower pH and nitric acid presence.

b) **Permanganic acid** (HP): HP involves utilizing a dilute solution (0.4-2mM) of $HMnO_4$ without additional additives commonly used in the CORD process. HP, being a potent oxidizing agent, tends to generate lower waste quantities due to its reduced concentration and the absence of specific ions (K^+, Na^+, and NO_3^-). The corrosion rate and decomposition of HP are also comparatively lower, possibly attributed to the absence of NO_3^-, which tends to promote metal corrosion [9]. HP can either be transported to the site or prepared on-site using $KMnO_4$ and cation IX resins. However, it's important to note that permanganic acid is inherently unstable, prone to decomposing into manganese dioxide (MnO_2), oxygen (O_2), and water (H_2O). Various factors, such as heat, light, and acids, can accelerate this decomposition reaction [39,40].

c) **Influence of UV light through a dynamic system**: In the traditional HP CORD D UV method, ultraviolet (UV) light is used to lower the redox potential of the solution, which in turn increases its corrosive properties [9]. As part of the ongoing research using the COREMIX process, there is a specific focus on examining the influence of UV light on this decontamination approach. The aim is to understand how the introduction of UV light may impact the overall efficiency and effectiveness of the COREMIX process, providing valuable insights into its potential benefits and limitations.

3.2.4   Other parameters

Other parameters were also identified, but were not extensively studied. They include:

1) **Flow rate of chemicals**: Adjusting the flow rate via the pump permits changes in the system's kinetics. Changes in the flow patterns of the chemical solutions can influence turbulence, thereby potentially affecting decontamination efficiency. However, testing this parameter necessitates a dynamic system and samples configured as flowing tubes, a setup not feasible in the present study due to constraints related to sample geometry.

2) **Temperature of solution**: Modifying the temperature of the solutions can improve process control and may impact overall operational expenses. While higher temperatures generally result in improved efficiency, they also come with increased energy consumption. Striking a balance is crucial, weighing the trade-off between energy input costs and efficiency gains. Safety measures

must be considered when surpassing the boiling point of the solution, usually set at 100°C. However, such adjustments were not possible in this study due to device limitations.

3) **Volume-to-surface area ratio (V/S)**: The volume-to-surface area ratio serves as a parameter for adjusting the solution volume within the decontamination system, with the goal of minimizing the total volume employed. The objective is to tune the solution volume to meet decontamination efficiency. Striking the right balance enables a reduction in the overall solution volume used during decontamination, consequently decreasing waste generation. This optimization enhances the efficiency of the decontamination method while minimizing resource consumption and waste production. In this study, this aspect was not explored extensively, as the initial volume selected was the minimum required to submerge the sample, accounting for the geometry after resin application.

3.3   Results on Chemical Decontamination using the COREMIX process

The chemical decontamination utilizing the COREMIX process was divided into two distinct stages. Initially, the process underwent optimization using the SS316 samples, which were prepared by SORC. Subsequently, the optimized process was implemented on the SS304L samples, which were prepared by NNL. This approach allowed for a systematic assessment and enhancement of the decontamination process, starting with one set of samples and then applying the optimized method to a different set of samples to evaluate its effectiveness across varying scenarios.

3.3.1   Optimization on SS316

The optimization process for the SS316 samples involved the systematic variation of the previously introduced parameters, with subsequent analysis of the efficiency for each set of conditions. This approach allowed for a thorough exploration of the impact of different parameters on the decontamination process. The efficiency analysis included evaluating the removal of the oxide layer and assessing the overall performance of the COREMIX process under diverse experimental conditions.

To validate the efficacy of oxide dissolution, the samples underwent another round of characterization using SEM-EDX and XRD. This additional analysis was conducted to confirm the effectiveness of the decontamination process, providing an assessment of the changes in the oxide layers on the sample surfaces.

3.3.2   Influence of chemical concentrations

The outcomes of the COREMIX process applied to the samples are depicted in Figure 14, showcasing cumulative concentrations of Cr, Fe, and Ni following three cycles of treatment. The results reveal that elevated concentrations of both potassium permanganate and oxalic acid contribute to increased efficiency in metal removal, evidenced by higher total metallic concentrations. Potassium permanganate demonstrates selectivity toward Cr oxidation, leading to higher Cr content after the permanganate step compared to Fe and Ni. Conversely, oxalic acid displays higher efficiency in dissolving Fe and Ni, with no significant increase in Cr release observed across the three samples after the oxalic acid step. This aligns with existing literature, emphasizing the need for an oxidative step using the COREMIX process to eliminate Cr oxides and a reductive step with oxalic acid for Fe and Ni oxides [9,41,42].
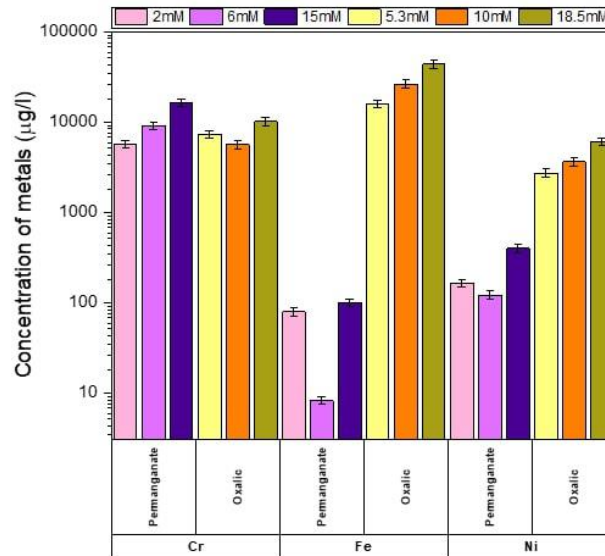
Figure 14 Concentration of metals detected in solution for three different combinations of potassium permanganate and oxalic acid after each stage

Additionally, the first two concentration combinations, 2mM $KMnO_4$ with 5.3mM oxalic acid and 6.3mM $KMnO_4$ with 10mM oxalic acid, require up to six cycles to completely remove the visible oxide layer, as illustrated in Figure 15.
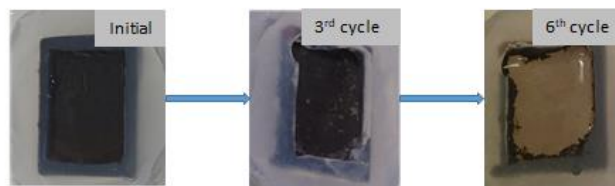
A. Evolution of sample treated at low concentrations (2mM $KMnO_4$ and 5.3mM $H_2C_2O_4$)
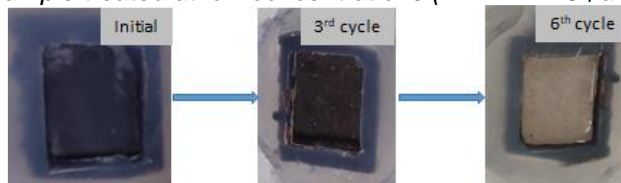
B. Evolution of sample treated at medium concentrations (6.3mM $KMnO_4$ and 10mM $H_2C_2O_4$)

C. Evolution of sample treat at high concentrations (15mM $KMnO_4$ and 18.5 mM $H_2C_2O_4$)

Figure 15 Surface evolution of samples treated at different concentration combination (a) Low concentration (2mM $KMnO_4$ and 5.3mM oxalic acid) (b) Medium concentration (6.3mM $KMnO_4$ and 10mM oxalic acid) and (c) High concentration (15mM $KMnO_4$ and 18.5mM oxalic acid)

3.3.3 Influence of contact time

The COREMIX process was replicated on a sample using the medium concentration combination of 6.3 mM KMnO4 and 10mM oxalic acid, but with an extended contact time of 6 hours per step, as opposed to the standard 4 hours. However, even with the increased contact time, it was observed

that, at this concentration combination, three cycles were insufficient for the complete removal of the oxide film, as depicted in Figure 16a. In a similar fashion, the process was reiterated using the high concentration combination of 15 mM $KMnO_4$ in 3 mM HNO_3, followed by 18.5 mM oxalic acid. The contact time for this iteration was reduced to 3 hours. Notably, despite the shorter contact time, the process demonstrated comparable efficiency, resulting in the complete removal of the visible oxide film after three cycles, as illustrated in Figure 16b.
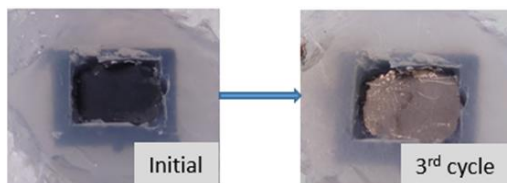
A. Sample treated at medium concentrations for 6 hours contact per step
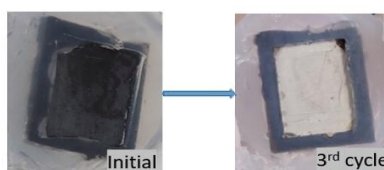
B. Sample treat at high concentrations for 3 hours contact per step

Figure 16 Surface evolution of samples treated at (a) Increased time of contact to 6 hours per step at medium concentration (6.3mM $KMnO_4$ and 10mM $H_2C_2O_4$) and (b) Decreased time of contact to 3 hours per step at high concentration (15mM $KMnO_4$ and 18.5mM $H_2C_2O_4$)

These results highlight that the refined chemical concentrations not only enhance the efficacy of the COREMIX process in eliminating oxide layers but also permit the optimization of treatment contact times. This optimization involves reducing the contact time per step to 3 hours, as opposed to the 4-6 hours commonly used in literature [9]. This adjustment is crucial for sustainability, as prolonged contact times at elevated temperatures would necessitate increased energy input, a significant factor influencing the environmental impact of the COREMIX process, as identified in the LCA studies.

3.3.4   Influence of oxidation step using HP in COREMIX

The optimized parameters of the COREMIX process were replicated through the application of the HP oxidation in COREMIX technique. Specifically, the conditions included the use of 15mM permanganic acid (HMnO4) for the oxidation step, followed by 18.5mM of oxalic acid for the decontamination step. This process was conducted over three cycles, maintaining a temperature of 80 °C for each step, with a duration of 3 hours for each step.

Figure 17 Evolution of the sample after 3 cycles of the HP oxidation during COREMIX process (15mM $HMnO_4$ followed by 18.5mM $H_2C_2O_4$), applied at 80°C for 3 hours/step

The incomplete dissolution of the oxide layer after three cycles is evident in Figure 17. Upon the introduction of oxalic acid, the occurrence of a white precipitate in the solution after approximately 30 minutes of contact indicated the degradation of oxalic acid, leading to suboptimal reduction in Ni-

Fe oxides. The presence of a black precipitate, MnO_2, on the sample's surface at the process's conclusion further supported the theory of oxalic acid reduction. MnO_2, a byproduct of the oxidation reaction, typically dissolves in oxalic acid. The poor performance of HP oxidation during the COREMIX tests, despite the anticipated enhancement in oxide film dissolution in theory [9], could be attributed to the elevated concentration of permanganic acid solutions employed—15 mM, compared to 6 mM in the literature [9]. At higher concentrations, permanganic acid solutions tend to exhibit increased instability [43].

3.3.5   Influence of UV light through a dynamic system

To investigate the impact of UV light on the optimized COREMIX process's efficiency, a straightforward dynamic loop system was devised, as depicted in Figure 18. The study utilized the optimized COREMIX process (15mM $KMnO_4$ in 3mM HNO_3 followed by 18.5mM oxalic acid, applied at 80°C for 3 hours/step). However, a temperature drop of approximately 20°C occurred in the decontamination chamber due to a lack of thermal isolation in the system. To address this temperature issue, the solution inside the reservoir tank was heated to a range of 90-95°C. Consequently, the solution in contact with the sample within the decontamination chamber reached a temperature of 72°C. Further heating was not feasible without reaching the boiling point.
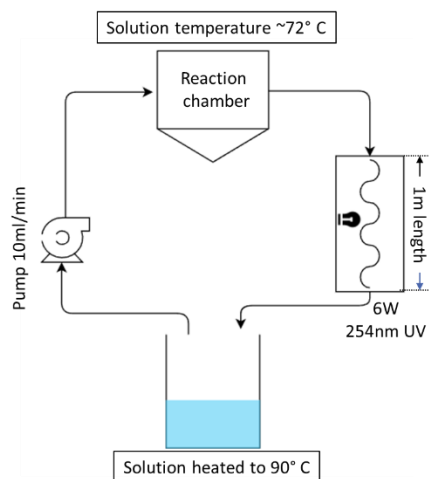

Figure 18 Simplified illustration of the laboratory loop setup

After the 3-hour $KMnO_4$ step, oxalic acid solution was introduced into the reservoir. UV light was activated following the addition of oxalic acid, with the solution passing through the UV chamber. During this process, a precipitate formed at the exit of the UV chamber as the sample returned to the reservoir tank. A black precipitate, MnO_2, generated as $KMnO_4$ reacted with Cr oxides, remained both inside the tank and on the sample as seen in Figure 19. This indicated that oxalic acid was unable to dissolve the MnO_2 precipitate. Additionally, a pH measurement indicated an increase in the pH level, reaching the range of pH 5, suggesting the degradation of oxalic acid. Figure 19 also shows the poor dissolution of the oxide film at the end of the three cycles.

Figure 19 Black precipitate on sample following application of the COREMIX loop with UV light with 15mM KMnO$_4$ in 3mM HNO$_3$ followed by 18.5mM oxalic acid, heated up to 95°C in the reservoir

Upon reviewing existing literature, a method for the degradation of oxalic acid using nitric acid and UV light, was described by Wang and Lum [44]. Their research indicated that UV light alone can effectively destroy oxalic acid in dilute nitric acid solutions. The authors found that UV photolysis of NO$_3^-$ generates OH$^-$, and this process is significantly accelerated at higher temperatures. Kubota also documented similar findings in their work [45]. Based on the observations made in this study and insights from F. Wang and B. Lum's work [44], it can be inferred that the UV light used in this investigation (254nm) is not compatible with the COREMIX process.

3.3.6 Post treatment Characterization

To assess the impact of the treatment procedure, a surface analysis was conducted on a post-treated stainless steel sample. As shown in Figure 20, the stainless steel sample, oxidized in 15g/L boric acid, underwent three cycles of the optimized COREMIX process.

In Figure 20A, the SEM image zooms in on the boundary between the treated and non-treated segments of the sample. The non-treated region, shielded by a silicon resin, is marked by the red line. The SEM image clearly indicates the absence of the oxide layer on the treated section, confirming the successful removal of the oxide film following the application of the optimized COREMIX process.

Further insights into the treated segment are provided by the EDX profile along the yellow dotted line in Figure 20B. A comparison of the EDX profiles between the treated and non-treated portions reveals the removal of the oxide layers. This underscores the high effectiveness of the optimized COREMIX process in dissolving the oxide layer after three cycles or 18 hours of contact.

The XRD analysis of the surface, as depicted in Figure 20C, aligns with the SEM and EDX findings. The reduction in the intensity of oxide peaks indicates a decrease in the presence of the oxide layer, accompanied by a relative increase in the peaks corresponding to the base metal. This serves as confirmation of the successful dissolution of the oxide film through the application of the optimized COREMIX process.
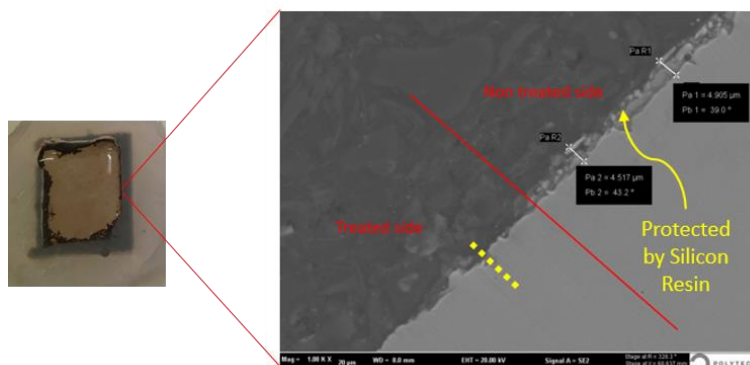
A. SEM image of the resin interface with markings made to distinguish the two sides
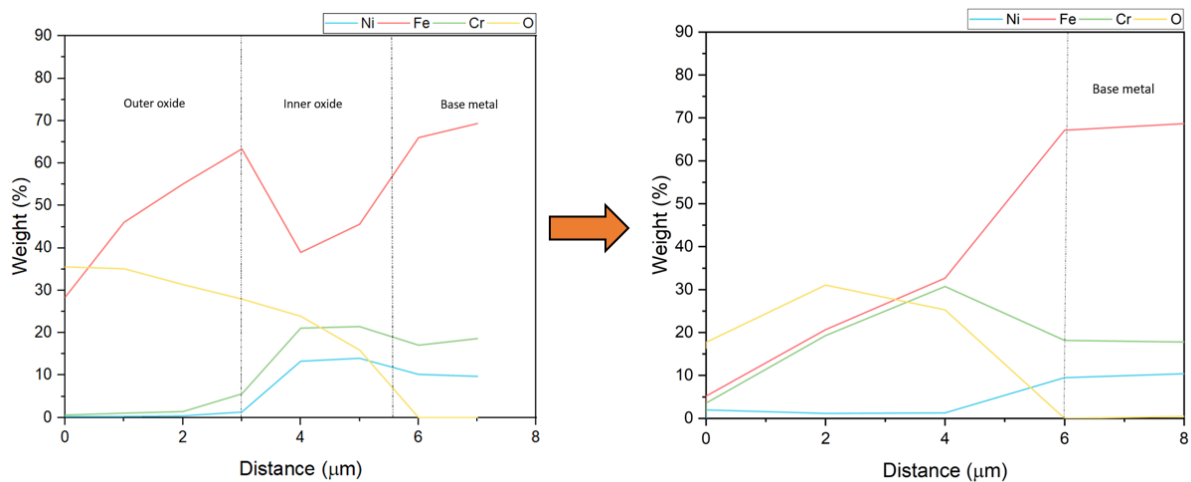
B. EDX profiles before (left) and after (right) treatment showing the removal of oxide layer
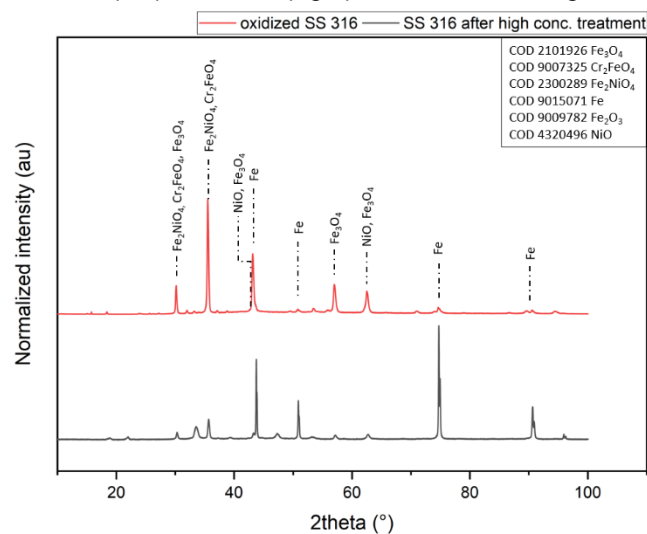
C. XRD profiles showing the decrease in intensity of oxide peaks

Figure 20 SEM, EDX and XRD profiles of a SS316 sample after treatment in comparison to protected oxide using resin; treatment using 3 cycles of optimized COREMIX process (15mM $KMnO_4$ in 3mM HNO_3 followed by 18.5mM oxalic acid, applied for 3 hours/step at 80°C)

3.3.7 Synthesis and Further Insights

The optimization of the COREMIX process targeted chemical concentration, contact time, and the influence of UV light. Due to equipment constraints and safety considerations, parameters such as solution volume, flow rate, and temperature were not extensively examined. Elevated chemical concentrations proved effective in reducing treatment cycles, enhancing decontamination efficiency. Oxalic acid played a pivotal role in completely eliminating the visible oxide film, particularly for Fe-Ni oxides, while $KMnO_4$ was crucial for oxidizing Cr oxides, essential for eliminating potential diffused activity. The optimal HNO_3 concentration was established at 3mM.

Based on these findings, an optimized COREMIX process was proposed: an oxidation step involving 3mM nitric acid with 15mM $KMnO_4$ at a V/S ratio of 0.4m, followed by the addition of a total of 44mM oxalic acid, with 18.5mM used for the reduction of Fe oxides in the decontamination step. The excess is employed to neutralize residual $KMnO_4$ and any MnO_2 precipitate formed during oxidation, particularly important for Ion Exchange (IX) resin applications. This optimized process, consisting of three 3-hour cycles at 80°C, effectively dissolved the oxide layer of stainless steel 316, validated by SEM-EDX and XRD studies. The resulting solution, containing metallic ions, could be efficiently

treated using methods like ion exchange resins or precipitation (COREMIX-HP). The precipitation protocol that can be applicable to the COREMIX process will be detailed in Deliverable 4.5.

The mass loss was estimated by weighing the samples before and after undergoing 3 cycles or 18 hours of treatment, resulting in a measured loss of 6.71 mg. This loss originated from the dissolution of the oxide layer on the exposed surface of the approximately 103 ± 0.0025 mm². To calculate the mass loss corrosion rate, the theoretical density value of SS316, 7.99 g/cm³ [46,47], was employed, given the complex and non-homogeneous nature of the stainless steel oxide layer. The calculated mass loss corrosion rate was 3.929 ± 0.074 mm/year or 0.449 ± 0.008 µm/h.

Significantly, this corrosion rate was notably higher than the rate reported by Jung et al. [38] for stainless steel 304L. In their study, oxalic acid (15.84mM) at 95°C for 20 hours resulted in a corrosion rate of approximately 0.005 µm/h [38]. It is crucial to acknowledge that their research focused on stainless steel 304L, known for its inherently higher corrosion rate due to its composition, in contrast to stainless steel 316 used in the present experiments. Stainless steel 316, characterized by enhanced corrosion resistance attributed to the inclusion of molybdenum in its composition [48–50], demonstrated a significantly increased corrosion rate through the optimized COREMIX process, thereby enhancing decontamination efficiency.

The optimized COREMIX process promotes environmental sustainability in the nuclear industry by reducing cycle frequency and contact times while increasing the corrosion rate. This not only saves time and resources but also minimizes effluent volume, thereby decreasing the environmental impact of the process.

3.4 Application on SS304L

The optimized COREMIX process was applied to samples prepared using boiling acid. In response to resin-related issues in initial tests, subsequent tests were conducted on the entire sample without resin. The solution volume was increased to maintain a consistent V/S ratio (0.4m) for comparability. Results revealed complete removal of the oxide surface after just one cycle, as depicted in Figure 21A. The mass loss for the entire sample was tracked through the three-cycle process, yielding a mass loss of 6.86 ± 0.06 mg. Estimating the corrosion rate using the density of SS304L, the rate was determined to be 0.555 ± 0.01 mm/y or 0.063 ± 0.001 µm/h. While this corrosion rate is lower than that of SS316 (0.449 ± 0.008 µm/h), it remains significantly higher than the rate reported by Jun Young Jung et al.[38] (0.005 µm/h) for SS304L using oxalic acid, indicating the superior efficiency of the optimized COREMIX process. The reduced corrosion rate can be attributed to the exceedingly thin oxide layer on these samples, which undergoes dissolution in the initial cycle. Subsequent cycles result in the dissolution of the base metal.

In the case of the next sample, the solution volume was reduced by approximately 50% in an effort to further minimize the required solution volume (Therefore a V/S of 0.18m). The application of the COREMIX process to resulted in the visible dissolution of the oxide layer after a single treatment cycle as seen in Figure 21B. The corresponding mass loss was 7.80 mg, leading to a corrosion rate of 0.586 ± 0.010 mm/y or 0.067 ± 0.001 µm/h, comparable to the sample with double the volume. Exploring additional volume reduction for SS304L samples resembling those found in reprocessing plants holds promise for high process efficiency. Unfortunately, further exploration of this prospect was constrained by the limited availability of samples.
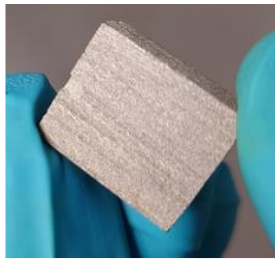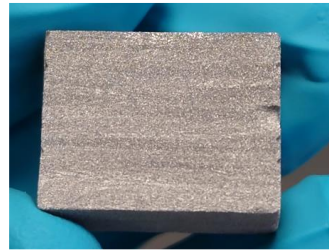
A. SS304L with V/S 0.4m   *B. SS304L with V/S 0.18m*

Figure 21 SS304L samples after 1 cycle treatment of COREMIX process (a) with V/S 0.4m and (b) V/S 0.18m.

The ICP-MS analysis across the two samples was carried out and categorized elements listed in Table 1 into groups based on their types: base metal elements (Cr, Fe, and Ni), lanthanides, transition elements, and "other elements." Elements such as N, Na, K, Al, and P were not measured due to ICP-MS incompatibility or instability during analysis, precluding their inclusion. The in-depth findings are available starting from section 3.3, page 107 in A. Rivonkar's thesis [51], while this report provides a general overview.

In general, base metal components (Cr, Fe, and Ni) exhibited trends similar to those observed in SS316, favouring Cr oxide oxidation in $KMnO_4$ and Fe and Ni oxide reduction in oxalic acid. The first cycle showed significantly higher metal release, with Cr, Fe, and Ni exhibiting higher concentrations in the initial cycle, indicative of effective oxide layer dissolution. The lanthanides, Nd, Sm, Gd, La, Ce, Pr, and Eu were detected, released exclusively during the oxalic acid stage after the first cycle, suggesting their presence in the oxide layers without penetrating the base metal surface. The transition elements and other elements were also found in the solution. Cs, Rb and Re exhibited release during the $KMnO_4$ stage, while other elements, including Ba, Sr, Y, Mo, Ru, Rh and Pd were released during the oxalic acid stage, predominantly in the first cycle.

Since the majority of dissolutions predominantly occur during the initial cycle, the subsequent cycles reveal the predominant presence of base metal components, Fe, Ni, and Cr. This observation serves to emphasize the remarkable efficiency of the oxide layer dissolution achieved within a single cycle of the optimized COREMIX process for such wastes. The rapid and effective removal of the oxide layer during the first treatment cycle is particularly noteworthy.

4 EASD® (Electrolytically Assisted Surface Decontamination)

4.1 Introduction

Electropolishing is a mature metal surface treatment technology that is commonly applied in a range of industrial applications, including in purification, post-weld treatments, and surface cleaning. This process is typically achieved by immersing a metallic item within a bath filled with a specific electrolyte. Electrical connections are then typically made to a direct current (DC) power supply. The targeted metallic item is connected to the positive electrical terminal (making it the anode) and a counter electrode is also located within the electrolyte, thus creating an electrochemical cell. Application of an electrical current facilitates the controlled dissolution of the anodic metal surface into the electrolyte. When this same process is applied to radioactive metallic waste items, the radioactive isotopes that have been incorporated into the surface material can also be removed, thus enabling waste reclassification and recycle of the bulk metal material.

In recent years, the UK's National Nuclear Laboratory (NNL) have conducted collaborative research with an electrochemical engineering company, C-Tech Innovation Ltd., to develop and patent an enhanced electropolishing methodology known as EASD® (Electrolytically Assisted Surface Decontamination) [52]. The goal of this technology development was to create flexible and controllable decontamination tools that could be deployed in-situ at nuclear sites during its decommissioning phase. An advantage of electrochemical decontamination is that can be utilised to enhance the effectiveness of native reagents already used at nuclear sites without the complications of adding new chemical agents, i.e., avoiding a limitation associated with chemical decontamination and the secondary waste challenges. Therefore, a secondary waste can be generated which is compatible with existing waste routes.

Several devices have been designed that incorporate this EASD® technology and enable the decontamination process to be applied to a range of items commonly identified as being contaminated during nuclear decommissioning programmes, e.g., pipework, tanks and hotspots on walls/floors. EASD® Gel is one technology variation that utilises a gel-based electrolyte, illustrated in Figure 22. This deployment option is most suited to scenarios where localised/specific areas of metallic surfaces or contamination 'hotspots' need to be decontaminated but limited effluent waste routes are available (e.g. a small, contaminated area on the base of an active glove box). Much of the development work linked with this technology has been performed in collaboration with Sellafield Ltd and the UK's Sellafield nuclear site in mind. The predominant chemical reagent used at this site is nitric acid, thus this has formed the basis of the electrolyte-media used in the EASD® Gel technology. However, the technology has been shown to be compatible with a variety electrolyte solutions and different metallic waste (e.g., stainless steels, nickel-alloys, lead etc.).
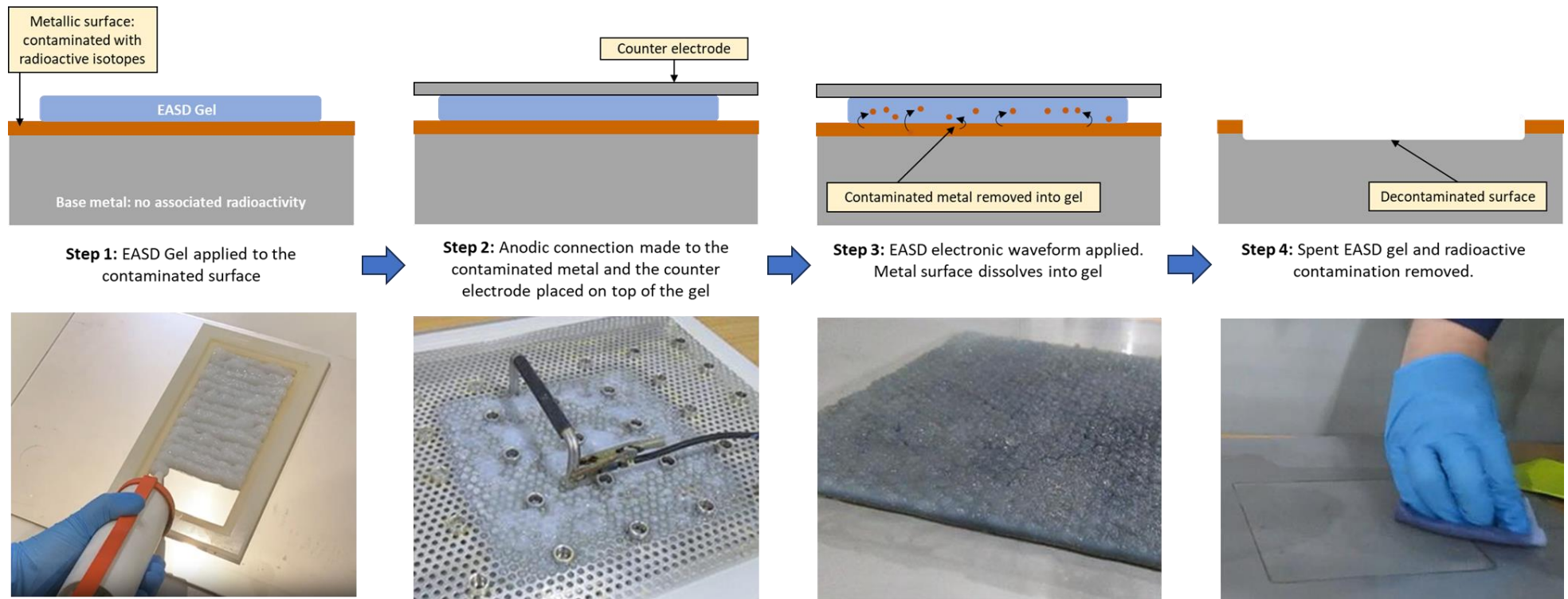
Figure 22: Diagram illustrating the EASD Gel process

4.1.1 Development performed during the PREDIS project.

Radioactive experimental testing and demonstration of the EASD® Gel technology was successfully completed prior to PREDIS project (Figure 23). The aim of the PREDIS project was to evaluate the technology's performance using the artificial nuclear-plant samples discussed in section 2, in parallel to the other innovations assessed as part of EU-project PREDIS, work package 4.
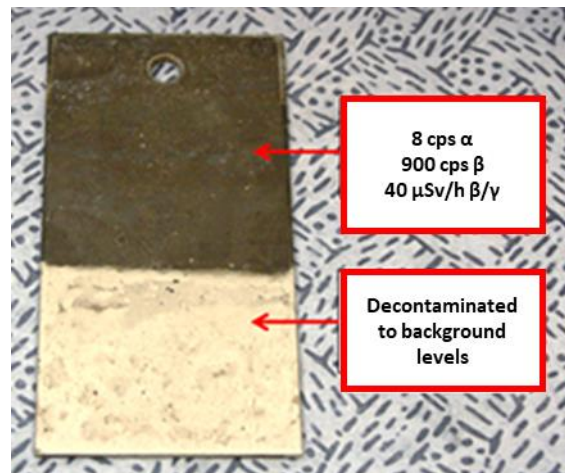

Figure 23: Image of a radioactive test coupon decontaminated via EASD® Gel

4.2 Methodology

Tests were conducted using the experimental set-up illustrated in Figure 24. A revised format compared to that shown in Figure 22 was required to accommodate the small size of the coupons (section 2). Test coupons were placed on a stainless steel sheet (50mm x 100mm) within a purpose-made plastic template. This template had the dual purpose of i) locating the coupon and ii) creating a void space above the coupon so that a 4mm thick layer of EASD® Gel could be applied. A meshed/perforated stainless steel sheet (50mm x 100mm) was then place on top of the gel, which acted as the counter electrode. This assembly was held together using a clamped arrangement and electrical connections were then made using crocodile clips.

The electrochemical decontamination process was controlled by the operator using the EASD® control panel, located at a distance from the items being decontamination. The control panel has a touch-screen interface which can be used to set the desired parameters (current/voltage). The applied electrical current (< 0.5 A/cm^2) was then operated by the on/off buttons. Limited to no decontamination of metal surface takes place when the electrical input is turned off. Once initiated, the EASD® control panel would automatically turn off the applied current after a specific programmed time interval. The EASD® Gel changes in colour (white to blue) and texture (increases in viscosity) during the decontamination process as the metallic ions are incorporated into the gel (Figure 22). At optimum surface removal rates, the gel reaches an operational performance limit at 45 minutes and needs to be removed. This was done using 2 spatula-type tools. Spent gel was stored in a plastic container prior to neutralisation and disposal.
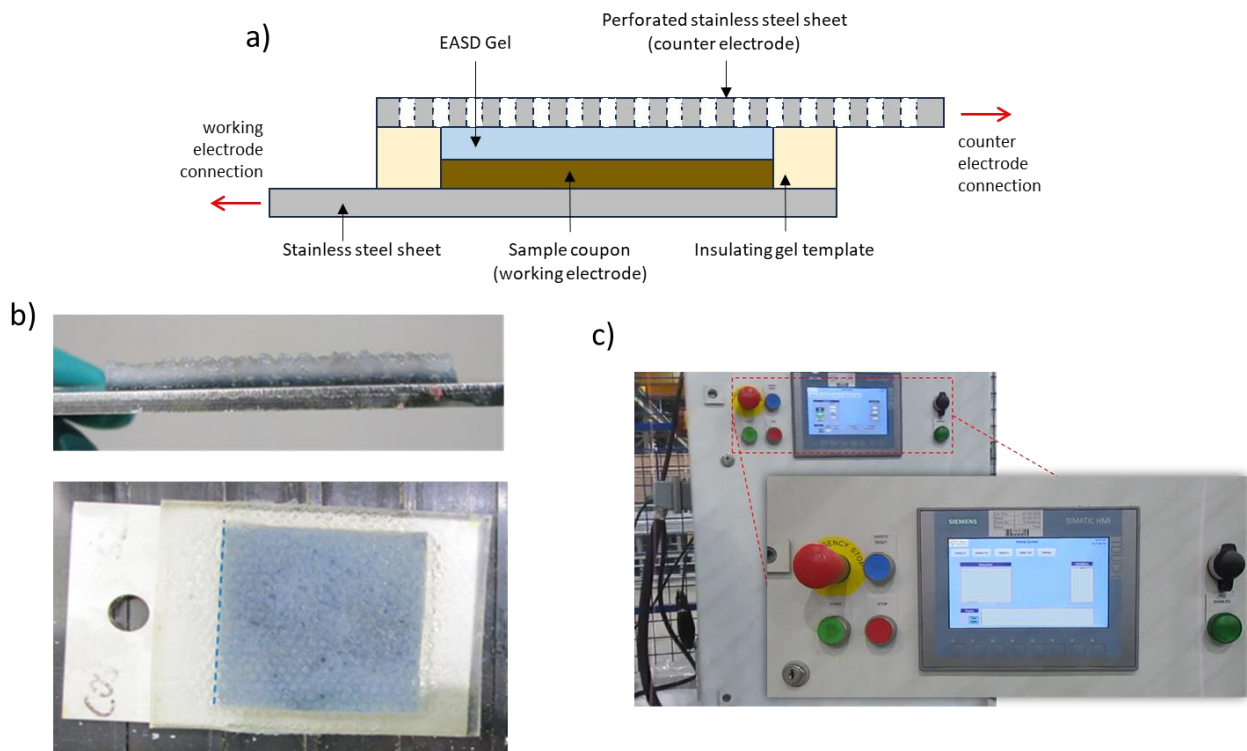
Figure 24: Images showing a) a schematic diagram and b) a photo representing the experimental set-up and c) the EASD® control panel.

4.3 Results

Table 3 shows images showing the 316Ti and 304L coupons before and after treatment via EASD® Gel. A significant difference in the visible appearance of the 316Ti coupons was observed post-treatment, changing from a dull grey/brown colour to a shiny silver. This was typical of a metallic oxide surface layer being removed and the bulk metal exposed. SEM image of the 316Ti coupons are shown in Table 5. Clear changes in the surface were observed, the rough metallic oxide being removed leaving a smoother 'electro-polished' surface post-treatment with the stainless steel grain boundaries visible. Up to 76 mg of surface material was removed from the 316Ti coupons, equating to a surface depth removal of ~25 μm. Surface removal rates achieved are detailed in Table 4. When compared to the characterisation data discussed on section 2.1, high decontamination of the coupons could be assumed as the removed surface material is in high excess of that expected to be contaminated.

A reduced visible difference in the 304L coupons was observed post-treatment, changing from a dull dark brown to a grey colour. Higher contrast was observed in the SEM images (Table 6). Up to 51 mg of material was removed from the 304L coupons, equating to a surface depth removal of ~9 μm. Slower surface removal rates were achieved when compared to prior work performed using 304L-grade stainless steel (typically 0.5 – 0.7 μm/min). This may have been caused by limitations in the small coupon geometry/experimental set-up. Despite this, high decontamination of the coupons would also be expected as the removed surface material is in high excess of the expected contaminated surface material (section 2.2).

Table 3: Images showing the 304L and 316Ti coupons before and after treatment via EASD® Gel

316Ti-grade coupons		304L-grade coupons	
Before	After	Before	After
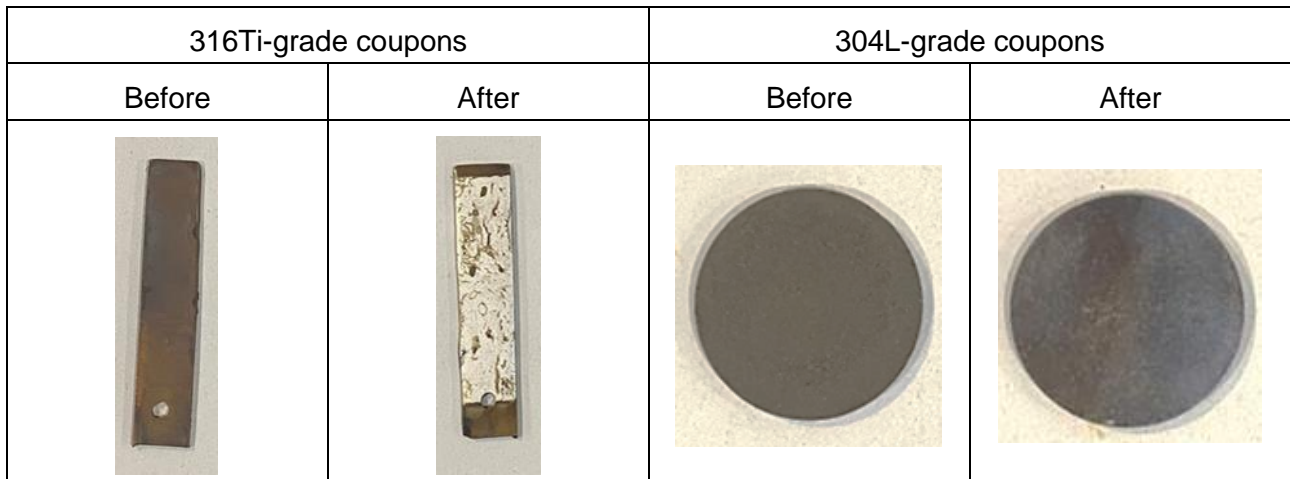
Table 4: Surface treatment data from the EASD® Gel

PREDIS coupon	Max. removal rate achieved (µm/min)	Max. removal rate achieved (mg/cm²/min)	Measured mass loss (mg)
304L-grade coupons corroded and contaminated in a high active liquor simulant	0.14	0.11	51
316Ti-grade coupons corroded under simulated PWR steam generator conditions	0.83	0.65	76

Table 5: SEM images of the SS316 coupons before and after EASD® Gel
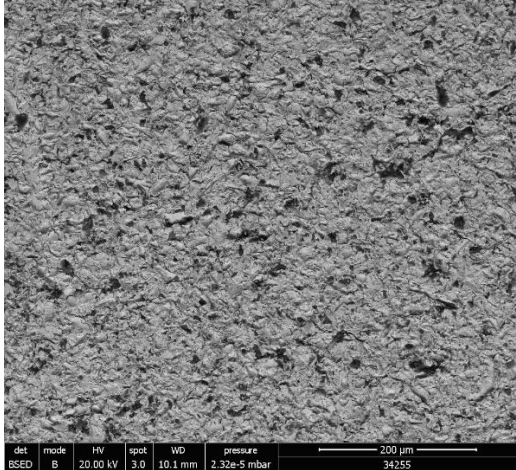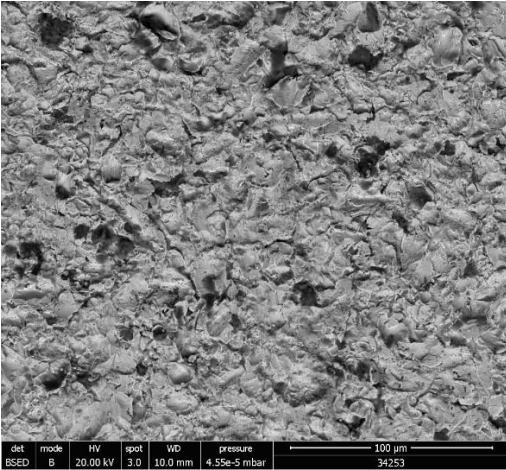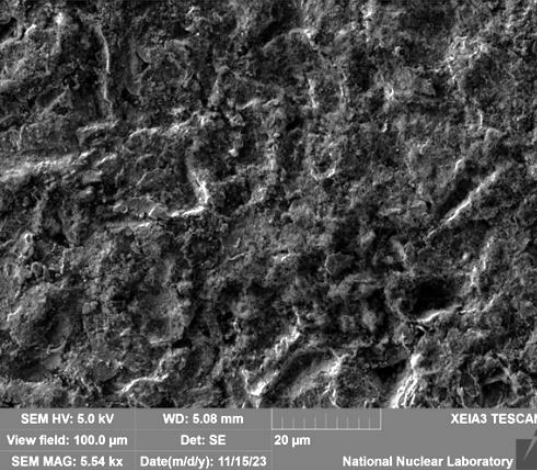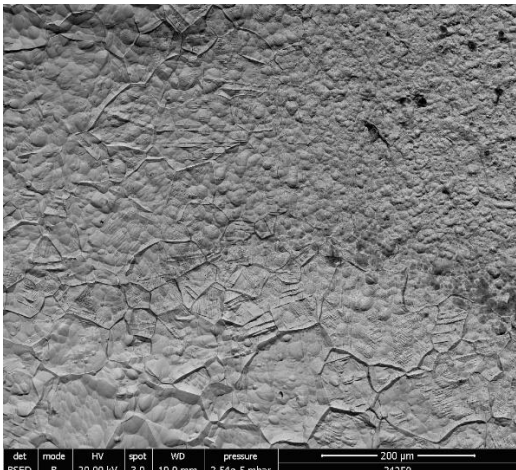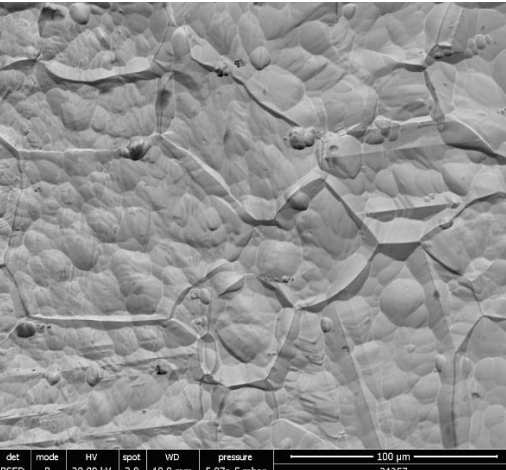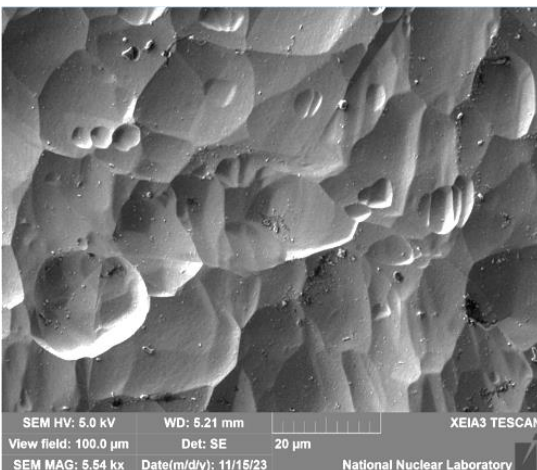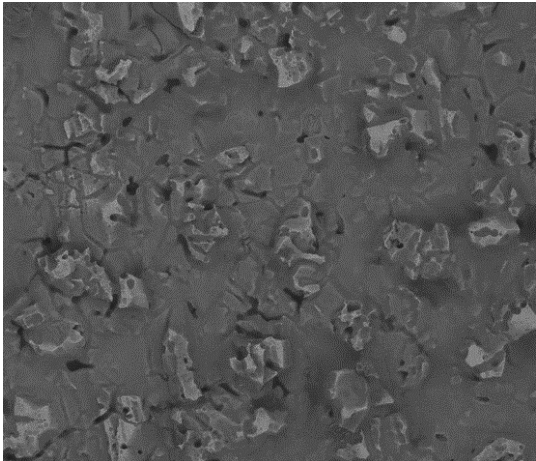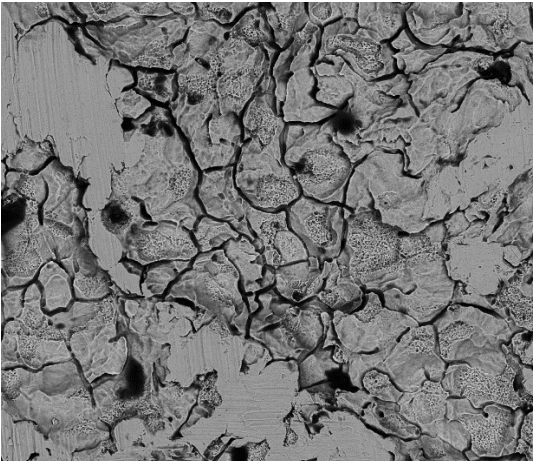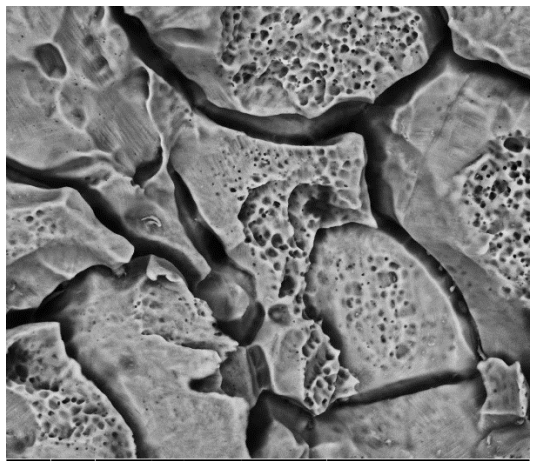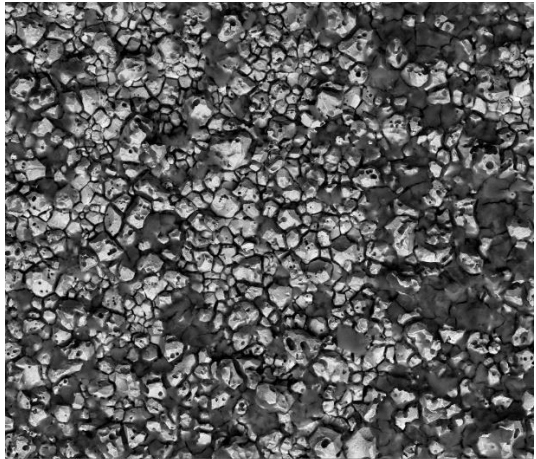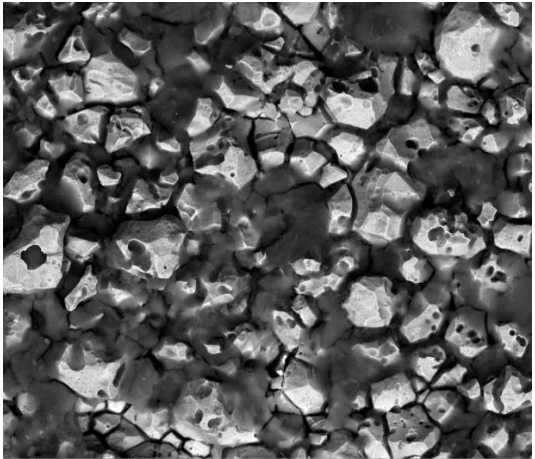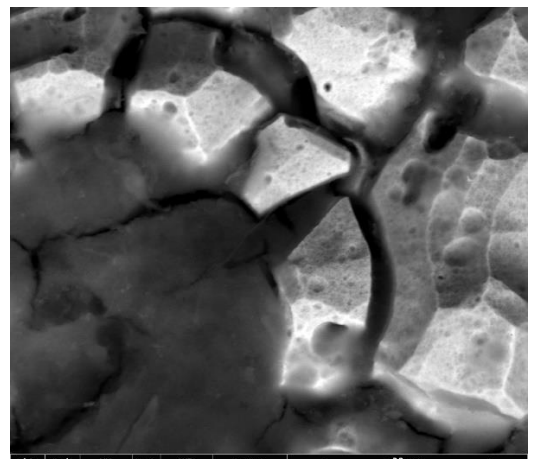
Table 6: SEM images of the SS304L coupons before and after EASD® Gel

5 Summary and perspectives

5.1 COREMIX process

The optimized COREMIX process reveals significant improvements and advantages for oxidized SS304L and SS316:

- **Improved decontamination efficiency**:
  - High chemical concentrations reduce treatment cycles and improve decontamination efficiency.
  - Oxalic acid is a key component: Complete elimination of visible oxide films, especially for Fe-Ni oxides.
  - $KMnO_4$ is a key player: oxidation of Cr oxides, essential for the elimination of potential diffused activity..
- **Reduction in treatment cycles**: high chemical concentrations have reduced the number of required treatment cycles, optimizing decontamination efficiency while saving time and resources.
- **Operational simplicity**: the process simplifies system setup by eliminating the need for specific resins in CORD reagent preparation and a UV source, resulting in significant cost and time savings.
- **Potential waste reduction**: the process, when combined with the precipitation process for effluent treatment, significantly reduces the volume of final waste generated, contributing to environmental sustainability.

The optimization of the COREMIX method has resulted in an increase in corrosion rate. However, this increase is actually a positive outcome as it indicates a reduction in the overall environmental impact of the decontamination process. Although the COREMIX process offers benefits, it has some limitations in the treatment of effluents rich in oxalic acid, an additional cleaning step with hydrogen peroxide is necessary. This additional step may increase the operational costs.

The optimized COREMIX process was used as a vacuumable gel, the methodology and results of which are fully presented and described in Deliverable 4.3. Here are mentioned the main outcomes:

- The vacuumable gel, formulated on the basis of COREMIX, shows high efficacy on surfaces with light to moderate oxidation, depending on the thickness of the oxide layer. Furthermore, the liquid bath COREMIX process is highly effective for substrates with significant oxidation.
- The COREMIX process is flexible and can be easily adapted to different oxide layer thicknesses by simply adjusting the number of treatment cycles. However, the liquid batch process requires delicate handling of concentrated chemical solutions. The use of gel overcomes this challenge, not only reducing the volume of liquid waste, but also reducing the need for post-treatment, thus minimizing the environmental impact. The COREMIX process uses subsequent precipitation methods to reduce waste volume and incorporate resins into a compatible conditioning matrix.

5.2 304L coupons

A detailed understanding of stainless steel surfaces contaminated under spent nuclear fuel reprocessing conditions was relatively unknown prior to this work. This project enabled a detailed methodology for preparing artificial coupons to be developed and atomic-scale resolution surface characterisation data to be collected. This was required due to the nano-metre thick oxides that form

in the oxidising nitric acid environment. Learning gained will provide key insight to stakeholders when decommissioning nuclear fuel-cycle facilities.

5.3 Electrolytically Assisted Surface Decontamination (EASD)

Electrochemical decontamination techniques can offer several advantages when compared with the more commonly applied chemical and mechanical decontamination technologies. Despite this, relatively few commercial technologies are available for decommissioning operations. Testing of the EASD® Gel in this work has enabled further technology development and demonstrated the fast decontamination capability it could offer, particularly for the in-situ for the treatment of radioactive hotspots. Testing of the technology using the artificial samples prepared for this work has demonstrated its capability further on a wider range of challenges in the nuclear sector.

6 Acknowledgements

REFERENCES

[1] Efremenkov, V. M., 1989, "Radioactive Waste Management at Nuclear Power Plants," IAEA Bull.

[2] World Nuclear Association, 2022, "Radioactive Waste Management | Nuclear Waste Disposal," Radioact. Waste Manag. [Online]. Available: https://world-nuclear.org/information-library/nuclear-fuel-cycle/nuclear-wastes/radioactive-waste-management.aspx. [Accessed: 07-Aug-2023].

[3] Slimák, A., and Nečas, V., 2016, "Melting of Contaminated Metallic Materials in the Process of the Decommissioning of Nuclear Power Plants," Prog. Nucl. Energy, **92**, pp. 29–39.

[4] ANDRA, 2018, "Inventaire National Des Matières et Déchets Radioactifs."

[5] Guo, X., Gin, S., and Frankel, G. S., 2020, "Review of Corrosion Interactions between Different Materials Relevant to Disposal of High-Level Nuclear Waste," Npj Mater. Degrad., **4**(1), pp. 1–16.

[6] Sadawy, M. M., and El Shazly, R. M., 2019, "Nuclear Radiation Shielding Effectiveness and Corrosion Behavior of Some Steel Alloys for Nuclear Reactor Systems," Def. Technol., **15**(4), pp. 621–628.

[7] Rodríguez, M. A., 2020, "Corrosion Control of Nuclear Steam Generators under Normal Operation and Plant-Outage Conditions: A Review," Corros. Rev., **38**(3), pp. 195–230.

[8] "Materials for Nuclear Engineering," Nucl. Power [Online]. Available: https://www.nuclear-power.com/nuclear-engineering/materials-nuclear-engineering/. [Accessed: 20-Jul-2023].

[9] Ocken, H., 1999, *Decontamination Handbook*, 112352, EPRI, Palo Alto, CA:

[10] McGrady, J., 2017, "The Effect of Water Chemistry on Corrosion Product Build-Up under PWR Primary Coolant Conditions," University of Manchester.

[11] Panter, J., Viguier, B., Cloué, J.-M., Foucault, M., Combrade, P., and Andrieu, E., 2006, "Influence of Oxide Films on Primary Water Stress Corrosion Cracking Initiation of Alloy 600," J. Nucl. Mater., **348**(1–2), pp. 213–221.

[12] Balbaud-Célérier, F., Gruet, N., Gwinner, B., and Laghoutaris, P., 2020, "Corrosion Behavior of Stainless Steels in Nitric Acid in the Context of Nuclear Fuel Reprocessing Plants," *Nuclear Corrosion*, Elsevier, pp. 301–340.

[13] Barton, D. N. T., Grebennikova, T., Denman, A. E., Carey, T., Engelberg, D. L., and Sharrad, C. A., 2023, "Long-Term Aqueous Contamination of Stainless Steel in Simulant Nuclear Reprocessing Environments," J. Nucl. Mater., **583**, p. 154551.

[14] Barton, D. N. T., Johnson, T., Callow, A., Carey, T., Bibby, S. E., Watson, S., Engelberg, D. L., and Sharrad, C. A., 2023, "A Review of Contamination of Metallic Surfaces within Aqueous Nuclear Waste Streams," Prog. Nucl. Energy, **159**, p. 104637.

[15] Callow, A., Connor, D., Carey, T., Summers, K., Hofer, C., Jusrkschat, K., Street, J., and Bibby, S., "Understanding the Hazard from Contamination on Nuclear Reprocessing Plant: A Study of Caesium and Strontium Uptake onto NAG18/10L Stainless Steel," Publ. Pending.

[16] Kerry, T., Banford, A. W., Thompson, O. R., Carey, T., Schild, D., Geist, A., and Sharrad, C. J., 2017, "Transuranic Contamination of Stainless Steel in Nitric Acid," **493**, pp. 436–441.

[17] Kerry, T., Banford, A. W., Thompson, O. R., Carey, T., Mosselmans, J. F., Ignatyev, K., and Sharrad, C. J., 2018, "Uranium Contamination of Stainless Steel in Nuclear Processing Plants," Ind. Eng. Chem. Res., **57**, pp. 3957–3962.

[18] Lang, A. R., Engelberg, D. L., Walther, C., Weiss, M., Bosco, H., Jenkins, A., Livens, F. R., and Law, G. T. W., 2019, "Cesium and Strontium Contamination of Nuclear Plant Stainless Steel: Implications for Decommissioning and Waste Minimization," ACS Omega, **4**(11), pp. 14420–14429.

[19] Alassali, A., Aboud, N., Kuchta, K., Jaeger, P., and Zeinolebadi, A., 2020, "Assessment of Supercritical CO2 Extraction as a Method for Plastic Waste Decontamination," Polymers, **12**(6), p. 1347.

[20] Ashtiani, R., Pullen, A., and Hammons, M., 2016, "Comparative Study of Water-Blasting Equipment for Airfield Surface Decontamination," J. Mater. Civ. Eng., **28**(8).

[21] Cavaghan, J., 2017, "Decontamination and Recovery of a Nuclear Facility to Allow Continued Operation," Radiat. Prot. Dosimetry, **173**(1–3), pp. 118–123.

[22] Kim, I.-T., 2013, "Fatigue Strength Improvement of Longitudinal Fillet Welded Out-of-Plane Gusset Joints Using Air Blast Cleaning Treatment," Int. J. Fatigue, **48**, pp. 289–299.

[23] Kohli, R., 2019, "Chapter 4 - Applications of Solid Carbon Dioxide (Dry Ice) Pellet Blasting for Removal of Surface Contaminants," *Developments in Surface Contamination and Cleaning: Applications of Cleaning Techniques*, R. Kohli, and K.L. Mittal, eds., Elsevier, pp. 117–169.

[24] Kumar, V., Goel, R., Chawla, R., Silambarasan, M., and Sharma, R., 2010, "Chemical, Biological, Radiological, and Nuclear Decontamination: Recent Trends and Future Perspective," J. Pharm. Bioallied Sci., **2**(3), p. 220.

[25] Máša, V., Horňák, D., and Petrilák, D., 2021, "Industrial Use of Dry Ice Blasting in Surface Cleaning," J. Clean. Prod., **329**, p. 129630.

[26] NEA, 2020, *Decontamination Techniques Used in Decommissioning Activities*, OECD Publishing, Paris.

[27] Wang, X., Li, J., Wang, L., Jia, X., Hong, M., Ren, Y., and Ma, M., 2021, "A Novel De-Rusting Method with Molten Salt Precleaning and Laser Cleaning for the Recycling of Steel Parts," Clean Technol. Environ. Policy, **23**(5), pp. 1403–1414.

[28] Zhong, L., Lei, J., Deng, J., Lei, Z., Lei, L., and Xu, X., 2021, "Existing and Potential Decontamination Methods for Radioactively Contaminated Metals-A Review," Prog. Nucl. Energy, **139**, p. 103854.

[29] Horváth D., 2017, "Development and application of multipurpose radiotracer methods for the investigation of sorption processes on structural material surfaces."

[30] Katona, R., Rivonkar, A., Locskai, R., Bátor, G., Abdelouas, A., Somlai, J., and Kovács, T., 2022, "Tafel-Analysis of the AP-CITROX Decontamination Technology of Inconel Alloy 690," Appl. Radiat. Isot., **181**, p. 110073.

[31] Salih, S., Gad-Allah, A., Abd El-Wahab, A., and Abd El-Rahman, H., 2014, "Effect of Boric Acid on Corrosion and Electrochemical Performance of Pb-0.08{\%} Ca-1.1{\%} Sn Alloys Containing Cu, As, and Sb Impurities for Manufacture of Grids of Lead-Acid Batteries," Turk. J. Chem., **38**, pp. 260–274.

[32] Zhang, S., Lu, Q., Xu, Y., He, K., Liang, K., and Tan, Y., 2018, "Corrosion Behaviour of 316L Stainless Steel in Boric Acid Solutions," Int. J. Electrochem. Sci., pp. 3246–3256.

[33] Machet, A., "Study of the initial stages of oxidation of stainless steels in high temperature water."

[34] Gault, B., Chiaramonti, A., Cojocaru-Mirédin, O., Stender, P., Dubosq, R., Freysoldt, C., Makineni, S. K., Li, T., Moody, M., and Cairney, J. M., 2021, "Atom Probe Tomography," Nat. Rev. Methods Primer, **1**(1), p. 51.

[35] "Decommissioning and Radioactive Waste Processing：Hitachi-GE Nuclear Energy, Ltd." [Online]. Available: https://www.hitachi-hgne.co.jp/en/activities/waste_treatment/index.html. [Accessed: 05-Apr-2023].

[36] Rivonkar, A., Katona, R., Robin, M., Suzuki-Muresan, T., Abdelouas, A., Mokili, M., Bátor, G., and Kovács, T., 2022, "Optimisation of the Chemical Oxidation Reduction Process (CORD) on Surrogate Stainless Steel in Regards to Its Efficiency and Secondary Wastes," Front. Nucl. Eng., **1**.

[37] Bertholdt, H. O., 1998, *HP/CORD D UV – A New Decontamination Process for Decommissioning of NPPs*, Report TR-110997, EPRI.

[38] Jung, J. Y., Park, S. Y., Won, H. J., Kim, S. B., Choi, W. K., Moon, J. K., and Park, S. J., 2015, "Corrosion Properties of Inconel-600 and 304 Stainless Steel in New Oxidative and Reductive Decontamination Reagent," Met Mater Int, **21**, pp. 678–685.

[39] Byers, H. G., 1899, "A Study of the Reduction of Permanganic Acid by Manganese Dioxide," John Hopkins University.

[40] Frigerio, N. A., 1969, "Preparation and Properties of Crystalline Permanganic Acid," J. Am. Chem. Soc., **91**(22), pp. 6200–6201.

[41] Wille, H., Bertholdt, H. O., and Roumiguiere, F., 1997, "Chemical Decontamination with the CORD UV Process: Principle and Field Experience," Slovenia.

[42] Balaji, V., Chandramohan, P., Rangarajan, S., and Velmurugan, S., 2018, "Dissolution of Nickel and Chromium from Ni-Cr-Fe-O Oxide by Oxidative Treatment with Permanganate," Prog. Nucl. Energy, **104**, pp. 136–142.

[43] 2020, "Permanganic Acid," Sci. Wiki [Online]. Available: https://www.sciencemadness.org/smwiki/index.php/Permanganic_acid. [Accessed: 20-Aug-2023].

[44] Wang, F., and Lum, B., 1995, "Photolytic Destruction of Oxalate in Aqueous Mixed Waste," Baltimore MD.

[45] Kubota, M., 1982, "Decomposition of Oxalic Acid with Nitric Acid," J. Radioanal. Chem., **75**(1), pp. 39–49.

[46] Material, W., 2019, "Weight & Density of Stainless Steel 304, 316, 316L & 303 in Lb/In3, g/Cm3, Lb/Ft3, Kg/M3," World Mater.

[47] Spira, N., 2021, "What Is the Density of Stainless Steel?," Kloeckner Met. Corp. [Online]. Available: https://www.kloecknermetals.com/blog/what-is-the-density-of-stainless-steel/. [Accessed: 24-Jul-2023].

[48] Sekine, I., Yuasa, M., and Yajima, H., 1997, "Corrosion behavior of various stainless steels in oxalic acid solutions and their corrosion resistance; Shusan yoekichu deno kakushu stainless ko no fushoku kyodo to sorera no taishokusei," Zair. Kankyo Corros. Eng., **46**.

[49] "304 vs 316 Stainless Steel: What Is the Difference? - Ryerson" [Online]. Available: https://www.ryerson.com/resource/the-gauge/grade-anatomy-stainless-304-vs-316. [Accessed: 24-Jul-2023].

[50] "SS304 Vs SS316, Difference Between 304 And 316 Stainless Steel-Materials" [Online]. Available: https://www.aluminum-flagpole.com/Materials/SS304-Vs-SS316-Difference-Between-304-316-Stainless-Steel.html. [Accessed: 24-Jul-2023].

[51] Rivonkar, A., 2023, "Optimization of Chemical Decontamination Methods for Radioactive Metals," IMT Atlantique.

[52] Collins, J., and Crawford, R., "Electrolytic Treatment for Nuclear Decontamination."